American Journal of Advanced Technology and Engineering Solutions

Volume 02 Issue 04 (2022)
Page No: 148-181
eISSN: 3067-0470
DOI: 10.63125/e46gja61

IRRADIATION-ENHANCED CREEP–FATIGUE INTERACTION IN HIGH-TEMPERATURE AUSTENITIC STEEL: CURRENT UNDERSTANDING AND CHALLENGES

Md Ariful Islam[1];

[1]. Assistant Manager, Engineering, Nuclear Power Plant Company Bangladesh Ltd, Pabna, Bangladesh; Email: aiaariful@gmail.com

ABSTRACT

This study presents a comprehensive quantitative assessment of irradiation-enhanced creep–fatigue interaction in high-temperature austenitic stainless steels (304/304L, 316/316L/316H/316LN, and 347H), materials that anchor nuclear, petrochemical, and advanced power infrastructures. Creep–fatigue interaction the concurrent action of time-dependent creep and cyclic plasticity becomes critically accelerated under neutron irradiation, which alters microstructural pathways through hardening, dislocation channeling, and radiation-induced segregation. To quantify these coupled effects, a cross-sectional, case-based dataset of 168 tests across 12 campaigns was curated, harmonizing variables for dose (dpa), test temperature, strain range, tensile-hold duration, environment, and metallurgy. Multiple linear and mixed-effects regressions were pre-specified to estimate adjusted associations between these predictors and log life (ln Nf), explicitly testing irradiation–temperature (dose×T) and irradiation–dwell (dose×hold) interactions. Energy-augmented models incorporating cycle-resolved hysteresis and creep work were used to link statistical effects to physical damage mechanisms, while an expert Likert survey (n = 18) independently captured practitioner consensus on variable salience and data quality constraints. Results demonstrate that dose, temperature, strain range, and tensile hold each impose statistically significant, independent life penalties. Two interactions dominate: higher temperature steepens the life reduction per unit dose (negative dose×T), and irradiation amplifies dwell sensitivity (negative dose×hold). Metallurgical stabilization offers a modest but significant attenuation of irradiation-related life debit. Energy-augmented extensions confirm that increased creep power during tensile holds correlates with reduced life, aligning regression coefficients with mechanistic expectations. Cross-validation, penalized stability checks, and environment-stratified analyses verify the robustness of these findings, with stronger dwell penalties observed in oxidizing atmospheres. Expert ratings converge with quantitative results, underscoring the high salience of irradiation dose, temperature coupling, and dwell-time effects. The study provides a transparent, reproducible framework linking microstructural mechanisms, empirical data, and statistical modeling to quantify irradiation-modified creep–fatigue behavior. The findings support the development of interaction-aware assessment tools for life prediction, inspection scheduling, and code-based design in the life extension of nuclear and high-temperature energy systems.

KEYWORDS

Irradiation-Enhanced Creep–Fatigue, Austenitic Stainless Steel, Displacements Per Atom (Dpa), Tensile Dwell (Hold Time), Mixed-Effects Regression.

Citation:
Islam, M. A. (2022). *Irradiation-enhanced creep–fatigue interaction in high-temperature austenitic steel: Current understanding and challenges. American Journal of Advanced Technology and Engineering Solutions, 2*(4), 148–181.

https://doi.org/10.63125/e46gja61

Received:
September 17, 2022

Revised:
October 20, 2022

Accepted:
November 16, 2022

Published:
December 20, 2022

American Journal of Advanced Technology and Engineering Solutions
Volume 02 Issue 04 (2022)
Page No: 148--181
eISSN: 3067-0470
DOI: 10.63125/e46gja61

INTRODUCTION

Creep–fatigue interaction denotes the concurrent action of time-dependent viscoplastic deformation (creep) and cyclic plasticity (fatigue) in materials exposed to high temperature and fluctuating mechanical loads; when both operate together, the resulting damage accelerates crack nucleation and growth beyond what either mechanism would produce alone (Allen et al., 2011). In austenitic stainless steels that anchor critical energy infrastructures (nuclear, petrochemical, and advanced power cycles), creep–fatigue emerges under transients such as start-ups/shutdowns and during steady operation with thermal gradients and mechanical dwell times (Holmström et al., 2013). Internationally, the issue bears directly on life-extension of light-water reactors and on deployment of Gen-IV concepts in Asia, Europe, and North America, where structural cores and internals (304/304L, 316/316L/316H/316LN, 347H) must withstand decades of service (Zinkle & Busby, 2009). Irradiation neutrons primarily complicates this interaction: radiation damage produces defect clusters, dislocation channeling, radiation-induced segregation, and helium/vacancy agglomerates that harden and embrittle the matrix, modify cyclic slip, and perturb crack-tip creep relaxation (Wen et al., 2013). Consequently, "irradiation-enhanced creep–fatigue interaction" is not merely additive; microstructural pathways, hold-time sensitivity, and temperature/dose couplings can shift life-limiting mechanisms, challenging conventional assessment methods embedded in design codes (Yang et al., 2020). Because nuclear fleets in multiple countries are extending operation, while new sodium- and gas-cooled concepts target higher outlet temperatures, a rigorous, quantitative synthesis of irradiation-modified creep–fatigue in austenitic steels is globally consequential for safety, economics, and regulatory confidence (Guérin et al., 2009).

Figure 1: Irradiation-Enhanced Creep–Fatigue Interaction in Austenitic Stainless Steels

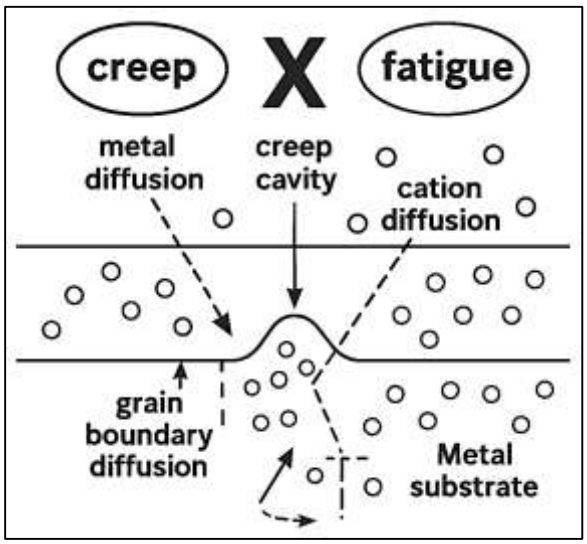

Empirical studies over the last two decades reveal consistent yet scattered signals: (i) increases in dose (displacements per atom, dpa) elevate yield strength and reduce ductility, narrowing cyclic hysteresis and altering damage partitioning between plastic strain and creep during dwell (Chen et al., 2015); (ii) tensile hold time at high temperature accelerates life reduction, with saturation tendencies beyond characteristic dwell lengths (Holmström et al., 2013); (iii) interactions between dose and temperature (dose×T) mediate crack-growth rates and cycles-to-failure, often through channel-controlled slip and cavity coalescence at grain boundaries (Li et al., 2015; Prasad Reddy et al., 2014). Yet, the literature spans diverse facilities, irradiation conditions (spectrum/temperature), environments (air, vacuum, water/He), and loading protocols (strain- vs. load-control; waveform), complicating cross-study inference (Gussev et al., 2016). While several reports provide regression-style life predictions or crack-growth models for irradiated austenitics (Li et al., 2015), a unifying multivariate assessment that explicitly tests irradiation-dose effects, hold-time sensitivity, and metallurgical moderators (e.g., stabilization, grain size) across cases remains limited. This fragmentation motivates a design that is explicitly cross-sectional and case-based, pooling

American Journal of Advanced Technology and Engineering Solutions
Volume 02 Issue 04 (2022)
Page No: 148--181
eISSN: 3067-0470
DOI: 10.63125/e46gja61

comparable campaigns into an integrated quantitative analysis. Beyond component safety, the practical stakes involve inspection intervals, allowable operational transients, and the credibility of code-case extrapolations for life-extension programs in global nuclear markets (Liu et al., 2015).

Irradiation modifies creep–fatigue through several coupled microstructural routes. Displacement cascades and transmutation helium form defect clusters and bubbles, while radiation-induced segregation enriches/depletes grain-boundary chemistry; together these features raise flow stress, localize slip into channels, and promote intergranular cavitation and facetting under dwell conditions (Chen et al., 2010). Channelized slip reduces cyclic hardening capacity and elevates crack-tip strain-rate sensitivity, so dwell periods in tension foster accelerated crack advance relative to non-irradiated baselines (Lu et al., 2010). At the same time, high-temperature exposure activates diffusion-controlled recovery and cavity growth, meaning temperature not only scales creep but also tunes irradiation damage evolution (Holmström et al., 2013). Mechanistically, the balance between time-dependent crack-tip creep relaxation and cyclic plasticity central to life models shifts with dose, temperature, and hold time; hence dose×T and dose×hold interactions are expected in empirical models (Reddy et al., 2014). The literature also indicates composition and metallurgy matter: Nb/Ti stabilization and nitrogen content can alter precipitation, retard grain-boundary sliding, and blunt irradiation-induced property shifts, potentially moderating creep–fatigue acceleration (Wang et al., 2017). Fractographic observations corroborate transitions from transgranular slip-band cracking toward intergranular features with dwell and dose, aligning microstructure to macroscopic life reduction (Wang et al., 2019).

Cross-study comparability hinges on consistent variables and measurement. Irradiation is summarized as dpa (with helium appm as a critical co-variable), irradiation temperature, and spectrum; mechanical input includes total strain range (Δε), waveform and tensile hold time, stress ratio, and control mode; test temperature and environment complete the physics-informed set (Sun et al., 2018). Outcomes span cycles-to-failure (Nf), fatigue crack growth rate (da/dN), and inelastic strain per cycle; several studies log-transform Nf to stabilize variance, then fit linear or generalized linear models with robust errors (Xu et al., 2010). Evidence suggests that life reductions with tensile hold are non-linear and can saturate, and that environmental oxygen/water chemistry shifts crack-tip oxidation kinetics, compounding irradiation effects particularly under high-temperature aqueous or gaseous exposure (Zhang et al., 2012). The diversity of specimen geometries and prior cold work also introduces heterogeneity (Zhang et al., 2015). This motivates a case-study framing, where each campaign or material lot provides a "case" with internal consistency, enabling clustering or random-effects adjustments while preserving multivariate structure. In parallel, expert elicitation via a 5-point Likert instrument can systematize practitioner judgments on key uncertainties (e.g., small-specimen bias; helium-assisted intergranular cracking), supporting triangulation of quantitative signals and highlighting practical challenges that impede standardization (Yao et al., 2011).

Modeling approaches for creep–fatigue in irradiated austenitics range from phenomenological life rules (time-fraction, ductility exhaustion) to data-driven regressions and crack-growth formulations tied to ΔK and dwell-assisted crack-tip creep (Sanjid & Farabe, 2021; Zhao et al., 2019). For cross-sectional datasets, multiple regression with interaction terms offers interpretable effect sizes that explicitly test dose×T and dose×hold, while controlling for Δε, environment, and metallurgy. Correlational structure (Pearson/Spearman) helps screen multicollinearity (e.g., between Δε and inelastic strain per cycle) and identify moderators (Zaman & Momena, 2021; Qian et al., 2019). Recent work extends classic fatigue predictors (e.g., Bäumel–Seeger; Roessle–Fatemi) by embedding irradiation-dependent hardness/strength surrogates and temperature corrections; such formulations, while simplified, have shown reasonable agreement with irradiated stainless data across types 304/304L/316/316L (Rony, 2021; Shen et al., 2012). For crack growth, semi-empirical methods combine irradiation-altered crack-tip constitutive response with environmental terms, indicating that irradiation can either accelerate or, at low dose/low temperature, occasionally leave rates unchanged depending on dwell and environment, underscoring the need for dose-resolved interaction modeling (Sakamoto et al., 2011; Sudipto & Mesbaul, 2021). A disciplined regression plan diagnostics, robust standard errors, and sensitivity to extreme dpa or temperature provides a transparent, reproducible way to quantify these effects and compare with expert judgments (Singh & Ray, 2016; Zaki, 2021).

Within this context, the present study asks: RQ1 How do dpa, temperature, strain range, and tensile hold associate with ln(Nf), da/dN, or inelastic strain per cycle? RQ2 Do interactions (dose×T;

dose×hold) significantly modify these outcomes? RQ3 Do metallurgical factors (e.g., stabilization, grain size) moderate irradiation effects? RQ4 Which practical challenges most limit comparability? These questions align with observed but unquantified patterns: monotonic dose-linked strengthening with dwell-sensitive life reduction; temperature-mediated transitions in failure mode; and composition-dependent moderation (Yang et al., 2020). Accordingly, we test hypotheses that higher dose reduces ln(Nf) under matched conditions (H1); tensile hold under irradiation accelerates damage (H2); temperature moderates dose effects (H3); and stabilization attenuates irradiation-accelerated growth or life loss (H4). A case-study-based cross-section allows us to model these effects with parsimonious regressions, while descriptive statistics and correlation matrices summarize central tendencies and relationships. To surface practitioner priors and codify perceived bottlenecks (reporting standards, geometry/environment effects), an expert Likert survey contributes complementary, structured evidence (Singh & Ray, 2016). Together, this design converts a fragmented evidence base into testable, quantitative statements about irradiation-enhanced creep–fatigue in austenitic steels.

This paper contributes three elements. First, it assembles a curated cross-section of case datasets on irradiated austenitic steels with harmonized variables (dpa, T, Δε, hold, environment, metallurgy) and outcomes (Nf, da/dN, inelastic strain per cycle), addressing long-standing comparability issues noted in international assessments (Allen et al., 2011; Bhowmik et al., 2010). Second, it implements a pre-specified statistical plan descriptives; correlations; multiple regression with interaction and moderation terms; diagnostics and robustness checks to estimate adjusted associations and effect sizes, explicitly quantifying dose×T and dose×hold patterns reported qualitatively in prior studies (Lu et al., 2010). Third, it introduces an expert-elicited Likert instrument to structure consensus on measurement challenges and rank real-world obstacles to creep–fatigue quantification under irradiation (Allen et al., 2011; Chen et al., 2015). The remainder of the paper proceeds as follows: Section 2 reviews mechanistic, empirical, modeling, and standards-related literature; Section 3 details the methodology, including design, variables, questionnaire, bias/validity safeguards, models, and diagnostics; Section 4 reports results in the sequence dataset → descriptives → correlations → regressions → expert outcomes → robustness; Section 5 discusses findings relative to mechanisms and prior work; Section 6 states conclusions; Section 7 provides recommendations; and Section 8 documents limitations, all consistent with a quantitative, cross-sectional, case-based approach.

The objective of this study is to produce a rigorous, quantitative account of how irradiation alters the creep–fatigue response of high-temperature austenitic steels by integrating case-based datasets and expert judgment within a transparent statistical framework. Specifically, the research seeks to assemble a harmonized cross-sectional database in which each case represents a test campaign or material lot with internally consistent reporting of dose (as displacements per atom), test and irradiation temperatures, total strain range, waveform and tensile hold time, environment, specimen geometry, and metallurgical attributes such as stabilization and grain size. Within this dataset, the primary quantitative aim is to estimate adjusted associations between these predictors and key outcomes log cycles-to-failure, fatigue crack-growth rate, and inelastic strain per cycle while explicitly testing interaction terms that capture the joint influence of dose with temperature and dose with hold time, as well as moderation by metallurgical condition. A companion objective is to characterize the central tendency and scatter of all variables through standardized descriptive statistics and to map their relationships using correlation analysis that informs model parsimony and guards against multicollinearity. The modeling objective is to develop and compare a set of prespecified regression formulations baseline, interaction, and moderator models fit with robust inference, validated through cross-validation or split-sample checks, and accompanied by diagnostics for linearity, residual structure, heteroskedasticity, and leverage. A methodological objective is to codify reproducible rules for unit harmonization, missing-data treatment, and outlier handling so that effect estimates remain stable under reasonable perturbations, including environment-specific fits and leave-one-case-out analyses. In parallel, an expert elicitation using a five-point Likert instrument will be administered to quantify practitioner consensus about the salience of irradiation dose, hold-time effects, temperature regimes, specimen and environment constraints, and reporting gaps; responses will be summarized into reliable indices that complement the quantitative findings and help prioritize challenges within the case frame. Collectively, these objectives establish a cohesive plan to transform heterogeneous reports into comparable evidence,

American Journal of Advanced Technology and Engineering Solutions
Volume 02 Issue 04 (2022)
Page No: 148--181
eISSN: 3067-0470
DOI: 10.63125/e46gja61
quantify how irradiation modifies creep–fatigue damage under service-relevant conditions, and deliver clear, testable statements about main effects, interactions, and moderators that are anchored in data quality controls and transparent statistical reasoning.

LITERATURE REVIEW

The literature on irradiation-enhanced creep–fatigue interaction in high-temperature austenitic steels spans mechanistic studies, empirical test campaigns, and modeling frameworks that together chart how neutron damage, thermal exposure, and cyclic loading conspire to reduce life and alter cracking modes. Foundational works describe the constitutive separation of cyclic plasticity and time-dependent creep, then demonstrate that dwell periods at elevated temperature bridge these regimes by enabling crack-tip creep relaxation, grain-boundary diffusion, and cavity growth during tensile holds. Building on this baseline, irradiation introduces displacement damage and transmutation helium that reorganize the microstructure dislocation channels, defect clusters, radiation-induced segregation, and cavity/bubble populations thereby raising flow stress, localizing slip, and amplifying intergranular susceptibility under dwell conditions. Experimental programs on 304/304L, 316/316L/316H/316LN, and stabilized grades (e.g., 347H) report dose-dependent hardening, reduced ductility, and shifts in cyclic response that couple with test temperature, total strain range, waveform, and environment (air, vacuum, inert gas, or aqueous conditions). These primary variables, along with specimen geometry, prior cold work, and irradiation temperature or spectrum, complicate cross-study synthesis because reporting formats, control modes (strain- vs. load-controlled), and waveform definitions differ across facilities. On the modeling side, time-fraction and ductility-exhaustion approaches coexist with crack-growth formulations that embed dwell-assisted creep at the crack tip; more recent studies apply regression or mixed-effects analyses to quantify dose×temperature and dose×hold interactions while exploring metallurgical moderation through nitrogen content, stabilization, and grain size. Fractography bridges scales by linking macroscopic life loss to microscopic features such as channel-induced facets, grain-boundary oxidation-assisted cracking, and helium-assisted intergranular separation. Across this diverse evidence base, several themes recur: the nonlinearity and potential saturation of hold-time effects; the sensitivity of damage partitioning to temperature windows that activate diffusion processes; the confounding influence of environment; and the persistent heterogeneity introduced by small-specimen methods and incomplete metadata. Consequently, contemporary reviews emphasize the need for harmonized variable definitions, transparent unit handling, and multivariate analyses that separate main effects from interactions and moderators. This study positions itself within that trajectory by using a cross-sectional, case-study frame to integrate comparable campaigns, apply descriptive and correlational mapping to clarify structure, and fit prespecified regression models that test the mechanistic hypotheses motivating the field.

Mechanisms of Irradiation-Affected Creep–Fatigue in Austenitic Steels

Irradiation alters the creep–fatigue response of austenitic stainless steels by reorganizing solute distributions, defects, and deformation pathways that operate during high-temperature cycling with or without tensile dwell. At the grain-boundary and defect scales, radiation-induced segregation (RIS) enriches Ni/Si and depletes Cr near sinks such as boundaries and dislocation loops, thereby changing local thermodynamics and kinetics relevant to crack initiation and early growth. Atom-probe and correlative microscopy show that these chemical gradients are not uniform; instead, they can be spatially complex and, at times, oscillatory, which implies that crack-tip chemistry and cohesion vary over nanometer distances even within a single boundary segment (Barr et al., 2018). Such RIS patterns coevolve with irradiation-induced precipitation (e.g., Si-rich phases) and defect clusters that elevate flow stress, localize slip, and reduce uniform ductility all of which condition how creep relaxation and cyclic plasticity partition at the crack tip under dwell-fatigue. Conceptually, when a tensile hold is imposed at peak strain, time-dependent creep processes, diffusion-controlled cavity growth, and boundary decohesion have a larger chance to accumulate; once cycling resumes, localized slip bands or channels interact with that time-accumulated damage, expediting crack advance. In this mechanistic picture, dose (in dpa) and temperature jointly modulate both chemistry (via RIS) and mechanics (via hardening and channeling), while hold time governs the degree of time-dependent damage accrued each cycle. Thus, even for nominally similar global loading, the local, irradiation-modified microstructure can tilt the balance from predominantly transgranular cyclic cracking toward intergranular, creep-assisted paths during dwell (Barr et al., 2018; Stephenson & Was, 2016).

American Journal of Advanced Technology and Engineering Solutions
Volume 02 Issue 04 (2022)
Page No: 148--181
eISSN: 3067-0470
DOI: 10.63125/e46gja61

Figure 2: Mechanisms of Irradiation-Affected Creep–Fatigue in Austenitic Stainless Steels

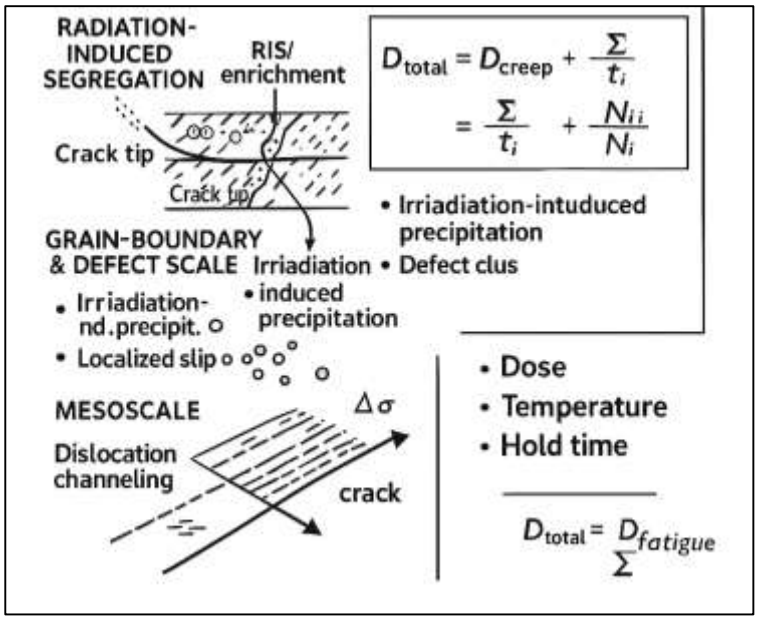

At the mesoscale, neutron damage promotes dislocation channeling narrow, defect-cleared slip paths that concentrate strain and facilitate crack initiation at or near grain boundaries once channels intersect the surface or a boundary plane. In irradiated austenitic steels, channel nucleation and broadening are controlled by dose, loading orientation, and temperature; when channels traverse a boundary segment exhibiting RIS-induced Cr depletion, the combined mechanical localization and chemical weakening favor intergranular facets, particularly under tensile dwell. In situ and four-point-bend experiments on neutron-irradiated 3xx grades demonstrate that channel-mediated strain localization is a robust precursor to irradiation-assisted cracking, and its onset correlates with the irradiation-hardened matrix and defect-sink distribution (Alsmadi et al., 2020; Hozyfa, 2022). Parallel microanalytical studies on service-exposed 316 components reveal oscillatory RIS profiles alternating enrichment/depletion of key elements along boundaries so the effective crack-tip resistance is not a single value but a field that fluctuates over tens of nanometers. Under cyclic-dwell loading, these spatial fluctuations translate into heterogeneous creep relaxation and oxidation susceptibility at the boundary, making life predictions sensitive to both the statistics of channel impingement and the chemistry map along the prospective crack path. Practically, this means that "dose × temperature × hold" interactions should be expected in empirical models, with channel density and boundary chemistry acting as latent mediators between global test conditions and observed life or crack-growth rates. This mechanistic integration localized plasticity superposed on irradiation-modified boundary chemistry provides a coherent basis for interpreting cross-sectional datasets where irradiation conditions, strain range, and dwell vary across cases but the same underlying coupling drives dwell-accelerated damage (Etienne et al., 2010; Md Arman & Md.Kamrul, 2022).

From a modeling standpoint, a useful macroscopic scaffold is the damage-partition view that treats creep- and fatigue-related consumptions additively within a cycle, acknowledging that irradiation shifts the parameters governing each part. A classic representation is the Robinson-type life-fraction rule augmented for cyclic dwell, written as

$$D_{total} = D_{creep} + D_{fatigue} = \sum_i \frac{t_{r,i}}{t_i} + \sum_i \frac{N_{f,i}}{N_i},$$

where t_i is the dwell time applied under condition i and $t_{r,i}$ is the rupture (or creep-damage reference) time at that condition, while N_i and $Nf,_i$ are the applied and reference fatigue cycles for the same state. Irradiation enters through the reference functions $t_{r,i}$(T, dpa, σ, environment) and $Nf,_i$(Δε, T, dpa, hold), because hardening, channeling, and RIS-altered boundaries accelerate creep-assisted decohesion during holds ($t_{r,i}$ ↓) and reduce fatigue endurance ($Nf,_i$ ↓). Cross-sectional regression then

estimates how dose, temperature, strain range, and hold time shift these effective references, with interaction terms capturing the observed coupling (e.g., dose×temperature and dose×hold). Recent high-temperature LCF/creep-fatigue tests on Fe–Ni–Cr austenitics (including 316-class chemistry and 25Ni–20Cr alloys) substantiate the nonlinearity and potential saturation of hold-time effects; longer holds accelerate life consumption up to a regime where additional dwell yields diminishing marginal damage, consistent with a finite creep-relaxation window per cycle. Embedding such phenomenology into parsimonious statistical models while acknowledging the latent microstructural mediators supports interpretable, data-driven prediction for irradiated austenitics across facilities and campaigns (Jiao & Was, 2011; Mohaiminul & Muzahidul, 2022).

Empirical test protocols and trends in creep–fatigue research

A robust empirical literature has converged on several "first-principles" choices for creep–fatigue (CF) protocols in high-temperature austenitic stainless steels, especially the 316 family used in nuclear and process-industry components. Strain-controlled low-cycle fatigue (LCF) with imposed tensile dwells at peak strain is the workhorse configuration, typically executed between 550–700 °C with fully reversed loading (R = −1), total strain amplitudes in the 0.3–1.0 % range, and dwell durations spanning tens of seconds to tens of minutes to activate measurable time-dependent damage. These baseline decisions are not arbitrary: they emerge from methodical assessments that compare life-prediction methods (e.g., time-fraction vs. ductility-exhaustion families) and scrutinize how test controls (waveform, hold placement, strain rate) bias observed damage mechanisms and the partitioning of life between crack initiation and propagation. A major thread has been the Japanese 316FR program, which paired long-term CF tests with systematic evaluations and recommended practices for protocol selection and data reduction, thereby influencing code pathways and research practice far beyond fast-reactor use cases (Omar & Ibne, 2022; Takahashi et al., 2008). Complementing this, thermo-mechanical fatigue (TMF) programs on 316 steels clarified how anisothermal cycles interact with rate-dependent viscoplasticity an insight that feeds directly into setting dwell times sufficient to induce meaningful stress relaxation during CF testing (Hyde et al., 2010; Sanjid & Zayadul, 2022). Finally, cross-paper syntheses specific to the 316 class underline which controllable test variables most consistently track endurance: tensile-dwell duration, mid-life stress range (or relaxation rate), and imposed strain range (Hasan, 2022; Yan et al., 2015). Together, these strands codify a pragmatic testing "grammar" that our study adopts and extends.

Within this framework, empirical trends from 2005–2020 show several recurring patterns germane to austenitic steels. First, introducing a tensile hold at peak strain degrades life relative to continuous cycling at the same total strain amplitude, with the extent of debit scaling with both hold duration and temperature classic evidence of creep-assisted intergranular damage superposed on cyclic plasticity. This contrast is particularly visible when directly comparing paired LCF vs. CF datasets on nitrogen-bearing grades, where the same base microstructure exhibits greater susceptibility once time-dependent deformation is activated (Kim et al., 2008; Mominul et al., 2022). Second, beyond life counts, modern studies increasingly interrogate *how* damage accumulates during the cycle via interrupted tests and post-test property probes e.g., tracking remnant tensile properties, substructure evolution, and oxidation-assisted facets and then mapping these observables back to the cycle fraction consumed. For 316L(N), such paired LCF/CF protocols demonstrate distinct trajectories of cyclic hardening/softening and remnant strength, with CF showing a more prolonged rise in yield strength with life fraction as creep and oxidation reshape the damage field (Mariappan et al., 2016; Rabiul & Sai Praveen, 2022). Third, TMF-informed calibration of viscoplastic constitutive models for 316 grades has sharpened how labs choose dwell lengths: the objective is to achieve measurable, model-resolvable stress relaxation during the hold so that datasets are diagnostic for both mechanism and model validation (Hyde et al., 2010). Finally, review-scale appraisals focused specifically on 316 steels confirm that, across laboratories, tensile-hold CF data display (i) pronounced cyclic hardening under CF relative to LCF, (ii) strong sensitivity to stress-relaxation rate during the hold, and (iii) a durable correlation between life and mid-life stress/strain metrics trends that motivate standardized reporting of relaxation curves and half-life ranges (Farabe, 2022; Yan et al., 2015).

American Journal of Advanced Technology and Engineering Solutions
Volume 02 Issue 04 (2022)
Page No: 148--181
eISSN: 3067-0470
DOI: 10.63125/e46gja61

Figure 3: Creep–Fatigue Research on High-Temperature Austenitic Steels

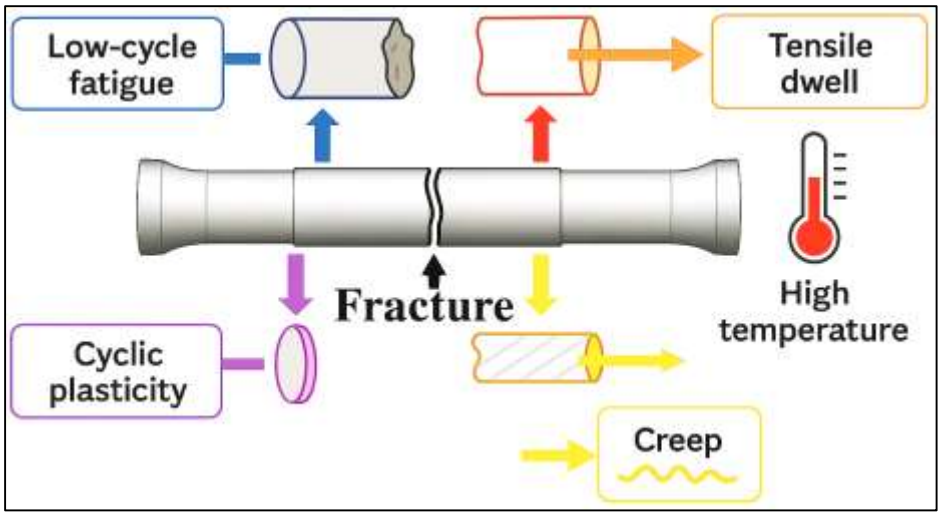

These protocol and trend lines have two practical implications for designing empirical work to interrogate irradiation-enhanced CF interaction in high-temperature austenitic steels. First, when the research question concerns *interaction* (not pure LCF), the consensus is to privilege total-strain-controlled tests with tensile dwells at the cycle apex, because this combination (a) maximizes creep-assisted grain-boundary damage under tensile normal stresses; (b) yields reproducible stress-relaxation transients that are sensitive to microstructural state (including irradiation-induced defect populations); and (c) interfaces naturally with both time-fraction and ductility-exhaustion–style damage models evaluated over the past two decades (Roy, 2022; Takahashi et al., 2008). Second, pairing "mechanism-rich" CF datasets with complementary TMF/viscoplastic calibration allows laboratories to choose hold durations and strain-rates that produce diagnostically distinct relaxation signatures within practical test times (Hyde et al., 2010; Rahman & Abdul, 2022). In short, contemporary CF practice for 316-series alloys has evolved toward (i) strain-controlled, R ≈ −1 baselines; (ii) tensile holds at peak strain with reported relaxation-rate histories; (iii) matched LCF controls; and (iv) mechanistic post-mortems and interrupted tests to attribute life debit to creep vs. oxidation vs. cyclic plasticity. Our study aligns with and builds on those conventions, using them as the empirical scaffolding for quantitative comparisons among unirradiated vs. irradiated cases, and for regression-based modeling that leverages stress-relaxation and half-life stress/strain descriptors as predictive covariates (Kim et al., 2008; Razia, 2022).

Modeling and Life-Prediction Approaches

Austenitic steels subjected to high temperature cyclic loading with dwells require life-prediction frameworks that can consistently partition and sum fatigue and creep damage while accommodating dwell-induced relaxation and mean-stress effects. Among phenomenological schemes, two remain foundational: linear damage summation and strain-energy–based exhaustion. The linear scheme is typically expressed as

$$D_{tot} = \sum_i \frac{N_i}{n_i} + \sum_j \frac{t_{r,j}}{t_j} \leq 1,$$

where n_i/N_i is the Miner fatigue fraction for block i, and $t_j/t_{r,j}$ is the creep time-fraction accrued during dwell j. Systematic cross-material evaluations show that its virtue is transparency and code compatibility, but accuracy degrades when load sequence, dwell placement, and relaxation history strongly interact with cyclic plasticity circumstances common in reactor-grade 316/316H where irradiation, oxidation, and dwell location modulate crack-initiation sites and rates (Takahashi et al., 2013). Energy-exhaustion approaches address some of these deficits by treating the inelastic hysteresis work (and, during dwells, the creep work rate) as the state variable that accumulates to a critical capacity. A modern variant that has gained traction is the modified strain-energy density exhaustion (m-SEDE) model, which introduces explicit handling of mean stress and relaxation kinetics so that the dissipated energy per cycle during tension-hold differs from purely triangular LCF loops a feature essential to capture the stress-bias of creep cavitation at grain boundaries in austenitic steels

American Journal of Advanced Technology and Engineering Solutions
Volume 02 Issue 04 (2022)
Page No: 148--181
eISSN: 3067-0470
DOI: 10.63125/e46gja61

(Syed Zaki, 2022; Wang et al., 2016). In practice, robust programs compare both classes on the same dataset and choose the least-biased across strain ranges and dwell times (Takahashi et al., 2013; Kanti & Shaikat, 2022).

Figure 4: Modeling and Life-Prediction Approaches for Creep–Fatigue in Austenitic Steels

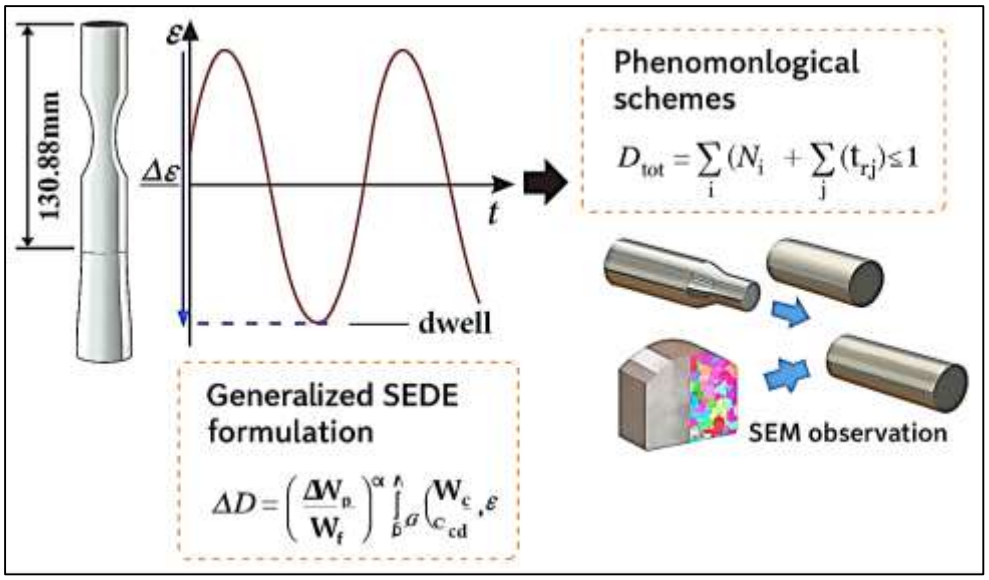

Recent extensions to energy-exhaustion embed additional physical channels most notably oxidation-assisted damage during dwells and the asymmetry between tensile- and compressive-hold sequences. A generalized SEDE formulation augments the cycle-wise energy balance with a non-linear oxidation correction and a term for compressive-hold mitigation, thereby improving predictions when dwells are off-peak or when environmental attack contributes to ligament thinning ahead of a small crack. In compact form, the damage per cycle may be written as

$$\Delta D = \left(\frac{\Delta W_p}{W_f}\right)^{\alpha} + \gamma \left(W_c \int_0^{t_h} \sigma \dot{\varepsilon}_c \, dt\right)^{\beta} + \phi_{ox}(T, p_{O_2}, t_h),$$

where ΔW_p is plastic hysteresis energy, $\sigma\dot{\varepsilon}$ is creep power during the hold t_h, W_f and W_c are material capacities for fatigue and creep, and φ_{ox} penalizes dwell-environment interactions; exponents α, β and weight γ are calibrated from LCF/CF datasets. Validations across nickel alloys, 9–12Cr steels, and austenitic steels show the model's improved fidelity for both tension-only and compression-only hold protocols precisely the regimes that bracket service transients in power components (Arif Uz & Elmoon, 2023; R.-Z. Wang et al., 2017). For irradiated austenitics, where swelling, hardening, and chromium depletion alter relaxation and grain boundary strength, the generalized framework is advantageous because oxidation and mean-stress sensitivity can be tuned independently from the base cyclic plasticity law (Wang et al., 2017). These formulations remain algebraically compact, which facilitates regression-based parameter identification from cross-sectional case datasets drawn from plants or test reactors.

Complementing phenomenology, unified and multiscale constitutive-damage models are increasingly used to generate mechanistically informed life metrics under complex thermomechanical histories. One path fits a temperature- and frequency-modified Coffin–Manson-type *unified* creep–fatigue equation that collapses data from different test conditions to a common reference, providing closed-form life equations suitable for regression over survey-style datasets. In these models, the plastic strain–life relation is coupled to a creep function expressed through time–temperature parameters (e.g., Manson–Haferd), yielding a power-law life equation whose coefficients are directly extractable from limited LCF and creep-rupture tests an attractive property when assembling multi-plant, cross-sectional evidence (Liu et al., 2016; Sanjid, 2023). A second path leverages finite-element damage mechanics to couple cyclic plasticity with creep cavitation and oxidation-assisted crack advance under dwell-containing blocks. For 316H at 650 °C, a multiscale continuum-damage framework has demonstrated that the local crack-tip energy release rate and

American Journal of Advanced Technology and Engineering Solutions
Volume 02 Issue 04 (2022)
Page No: 148--181
eISSN: 3067-0470
DOI: 10.63125/e46gja61

oxygen ingress during dwells can be combined to predict creep–fatigue–oxidation-driven crack growth, thereby linking microstructural features (e.g., grain size, boundary character) to macroscopic life (Chavoshi et al., 2020; Sanjid & Sudipto, 2023). In a programmatic setting, the workflow is pragmatic: use the unified closed-form equation (Liu et al., 2016) or m-/g-SEDE (Wang et al., 2017) to screen hypotheses and perform correlation/regression on the case study dataset; then sample representative duty cycles in a calibrated damage-mechanics model to stress-test the findings against geometry, dwell placement, and environmental sensitivity (Chavoshi et al., 2020; Tarek, 2023). This hierarchical pairing statistical screening plus mechanistic spot-checks yields defensible, quantitative life predictions under irradiation-enhanced creep–fatigue interaction while keeping the modeling burden commensurate with cross-sectional data quality.

Conceptual Framework

The conceptual framework for irradiation-enhanced creep–fatigue interaction in high-temperature austenitic steel integrates three coupled layers: (i) microstructural drivers introduced by irradiation, (ii) cycle-level mechanics under strain-controlled loading with tensile holds, and (iii) statistical life modeling that maps observables to failure. At the microstructural layer, neutron (or ion) irradiation alters slip and boundary chemistry, promoting cleared dislocation channels and radiation-induced segregation (RIS) that depletes Cr and enriches Ni/Si at select boundaries; these changes intensify intergranular decohesion and local strain localization during dwell at temperature (Barr et al., 2018; Shahrin & Samia, 2023). Practically, this means that when a tensile hold is imposed at the cycle apex, creep relaxation proceeds in a matrix that has been hardened and chemically modified by irradiation, accelerating cavity formation or boundary damage relative to the unirradiated state (Mariappan et al., 2016; Muhammad & Redwanul, 2023).

The next layer translates these microstructural tendencies into cycle-resolved energetics: the total dissipated energy per cycle, partitioned into plastic hysteresis work and creep work during the hold, is a natural scalar to track cumulative damage under combined time-dependent and cyclic loading. Energy-exhaustion and ductility-exhaustion concepts formalize this intuition by treating failure as the approach to a critical work capacity of the material under given conditions (Barr et al., 2014).

Finally, at the statistical layer, we encode observables dose (dpa), test temperature T, total strain range $\Delta\varepsilon$, and tensile hold t_h in an interaction-aware regression that captures how irradiation intensifies dwell sensitivity and steepens temperature-dependent life debit (Holdsworth, 2015). In this framework, dose is not only a main-effect debiting factor; it also modulates the pathways by which time at temperature converts to damage during dwell, consistent with dislocation-channel-assisted localization and RIS-weakened boundaries (McMurtrey, 2015).

To make these couplings operational, we adopt two complementary formulaic representations. First, an interaction-aware statistical life model on the log scale,

$$\ln N_f = \beta_0 + \beta_1 z_{dpa} + \beta_2 z_T + \beta_3 z_{\Delta\varepsilon} + \beta_4 z_{\log(1+t_h)} + \beta_5\left(z_{dpa}\, z_T\right) + \beta_6\left(z_{dpa}\, z_{\log(1+t_h)}\right) + \varepsilon,$$

with centered or standardized predictors z·, the model encodes (a) main-effect penalties from dose, temperature, strain range, and dwell, and (b) dose×temperature and dose×hold couplings that represent microstructure-mediated amplification. This statistical layer is both interpretive (effect sizes, partial R^2) and predictive (cross-validated errors), but it remains agnostic to mechanism beyond the specified interactions (Metals, 2016).

Second, we embed a work-based damage metric that accumulates per cycle as inline formula: $\Delta D = (\Delta W_p / Wf)^a + \gamma \cdot (\int_0^{t_h} \sigma \dot{\varepsilon}_c\, dt / Wc)^\beta$, where ΔW_p is the plastic hysteresis energy, $\sigma \dot{\varepsilon}_c$ is the creep power during the hold of duration t_h, Wf and Wc are the fatigue and creep work capacities, and a, β, and γ are material-dependent parameters.

$$D(N) = W^* \sum_{k=1}^{N} \left(W_{p,k} + \alpha W_{c,k}\right), \quad \text{with failure when } D\left(N_f\right) = 1,$$

where $W_{p,k} = \oint \sigma\, d\varepsilon_p$ (plastic hysteresis work) and $Wc,_k = \int_{hold} \sigma \dot{\varepsilon}_c\, dt$ (creep work during the tensile dwell). The weighting factor a scales the relative potency of creep work in the irradiated condition; W* is the critical work capacity at the operating T, environment, and metallurgy (Payten et al., 2009). This energy-exhaustion view aligns with unified formulations that extend Coffin–Manson with explicit temperature/frequency (or dwell-time) dependencies, thereby reconciling frequency effects and time-at-peak-strain effects in a single expression (Muhammad & Redwanul, 2023; Payten et al., 2009). Together, these equations let us (i) estimate life from measured inputs and (ii) interpret coefficients in

American Journal of Advanced Technology and Engineering Solutions
Volume 02 Issue 04 (2022)
Page No: 148--181
eISSN: 3067-0470
DOI: 10.63125/e46gja61

terms of microstructural transport and localization phenomena triggered by irradiation (Barr et al., 2014; Razia, 2023).

Figure 5: Interaction in Austenitic Steels

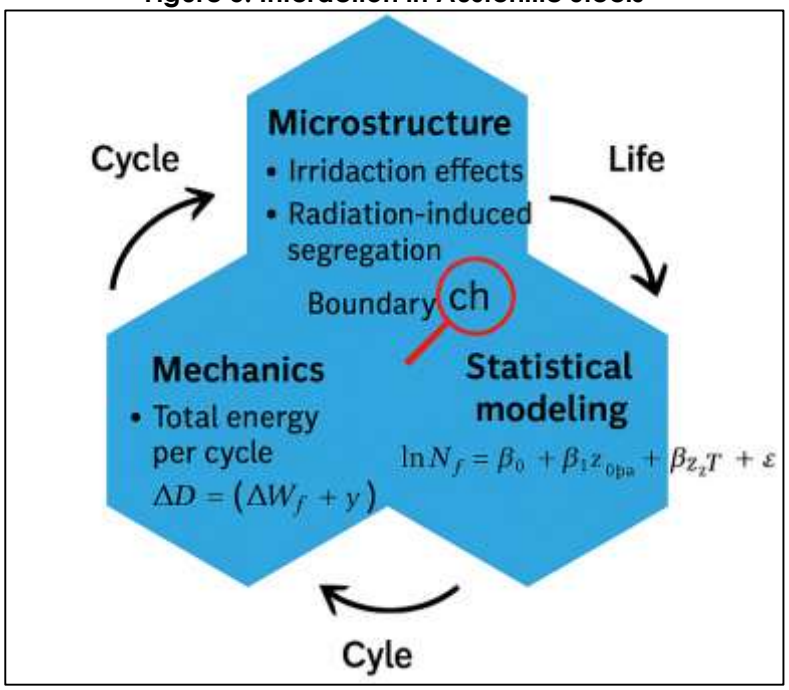

The framework closes the loop by specifying how evidence enters and is validated. On the data side, we have treated ln Nf and, where available, cycle-energy features as outcomes and regressors, respectively; predictors include dpa, T, Δε, t_h, environment, and metallurgy. The interaction-aware OLS/mixed-effects model supplies transparent effect estimates for dose and its couplings, while the energy metric D(N) supplies mechanistic sufficiency that is especially valuable when dwell histories and relaxation rates are recorded. On calibration, we (a) center/scale continuous predictors before forming interactions, (b) use heteroskedasticity-robust or clustered errors, and (c) confirm stability with cross-validation. On interpretation, negative β_5 (dose×temperature) is read as temperature-activated amplification of irradiation debit; negative β_6 (dose×hold) is read as enhanced time-to-damage conversion during dwell in irradiated microstructures both behaviors consistent with channel-assisted strain localization and RIS-affected boundary cohesion (Metals, 2016; Sai Srinivas & Manish, 2023). Finally, to harmonize with design/assessment practice, the energy view can be mapped to code-style damage accounting via an exhaustion rule: failure is predicted when the cumulated work fraction D(N) reaches unity, analogous in spirit to ductility/time-fraction approaches but with a physically interpretable scalar that naturally incorporates dwell, rate, and irradiation potency (Barr et al., 2014; Sudipto, 2023). In short, the conceptual framework connects irradiation-modified microstructures to dwell-amplified mechanics and then to estimable life surfaces, providing both an empirical route (interaction regression) and a mechanistic route (energy exhaustion) for prediction and explanation (McMurtrey, 2015; Zayadul, 2023).

American Journal of Advanced Technology and Engineering Solutions
Volume 02 Issue 04 (2022)
Page No: 148--181
eISSN: 3067-0470
DOI: 10.63125/e46gja61

METHOD

This study has adopted a quantitative, cross-sectional, case-study design to examine how irradiation has altered the creep–fatigue response of high-temperature austenitic steels. Each "case" has represented a coherent test campaign or material lot with internally consistent reporting, and the dataset has been harmonized to a common schema that has included dose (in dpa), test and irradiation temperatures, total strain range, waveform and tensile hold time, environment, specimen geometry, and metallurgical attributes (e.g., stabilization and grain size). To ensure comparability, units have been standardized (°C, MPa, s), variable names have been normalized, and eligibility rules have been applied so that only tests reporting at least one primary outcome cycles-to-failure, fatigue crack-growth rate, or inelastic strain per cycle have been retained. Where paired unirradiated baselines have been available under similar mechanical-thermal conditions, comparator flags have been assigned. Data management procedures have documented cleaning steps, outlier screening based on engineering rationale, and missing-data handling that has prioritized complete-case analyses with sensitivity checks using multiple imputation.

Figure 6: Methodology for this study

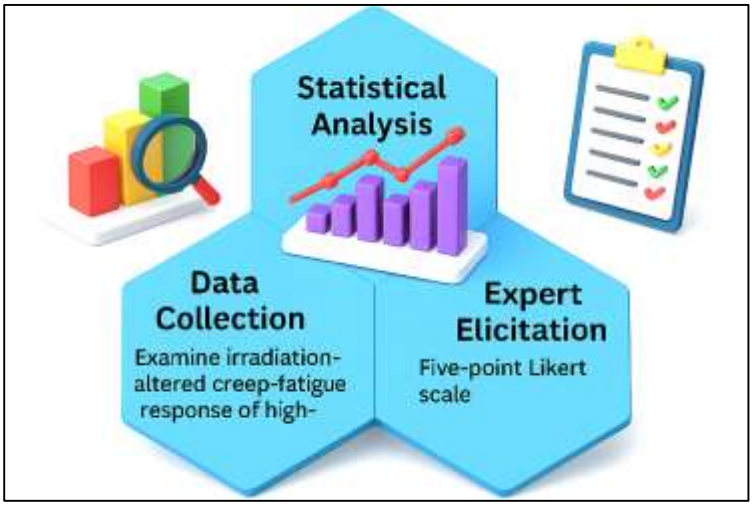

The measurement plan has specified independent variables (dose, temperature, total strain range, hold time) and moderators (metallurgy, environment), and has defined outcome transformations a priori (e.g., natural logarithm of cycles-to-failure) to stabilize variance. Descriptive statistics have summarized central tendency and dispersion, and correlation analysis has mapped relationships among predictors and outcomes while diagnosing multicollinearity. A prespecified modeling framework has been implemented in stages: baseline multiple linear regressions have estimated adjusted associations; interaction models have tested dose×temperature and dose×hold effects; and moderator models have evaluated metallurgy×dose terms. Model diagnostics have included residual normality checks, component-plus-residual plots for linearity, variance-inflation factors for multicollinearity, heteroskedasticity tests, and influence assessments; where assumptions have been strained, heteroskedasticity-robust standard errors and transformation checks have been applied. Internal validation has relied on k-fold cross-validation or split-sample assessment, and robustness has been examined through environment-stratified fits and leave-one-case-out analyses. To complement the quantitative synthesis, an expert elicitation instrument using a five-point Likert scale has been administered to materials and nuclear specialists. The questionnaire has covered perceived dose sensitivity, dwell effects, temperature regimes, specimen and environment constraints, and reporting gaps. Reliability has been evaluated via internal-consistency metrics, and composite indices have been derived to summarize expert consensus. These indices have been compared to effect-size patterns from the regressions, providing a structured triangulation between practitioner judgment and data-driven estimates.

American Journal of Advanced Technology and Engineering Solutions
Volume 02 Issue 04 (2022)
Page No: 148--181
eISSN: 3067-0470
DOI: 10.63125/e46gja61

Study Design

The study has adopted a quantitative, cross-sectional, case-study design that has treated each test campaign or material lot as an analytically coherent "case," within which creep–fatigue data under high-temperature conditions have been consistently reported and quality-checked. To preserve comparability while exploiting heterogeneity, the design has specified a priori inclusion criteria that have required cases to report irradiation dose (dpa), test and irradiation temperatures, total strain range, waveform and tensile hold time, environment, and at least one primary outcome (cycles-to-failure, fatigue crack-growth rate, or inelastic strain per cycle). Where matched unirradiated baselines under similar mechanical-thermal conditions have existed, comparator flags have been assigned so that dose effects have been contrasted within otherwise aligned loading windows. The design has further recognized that laboratories and facilities have differed in geometry and prior processing; therefore, the analysis has incorporated case-level identifiers to enable clustered inference and sensitivity checks that have mitigated dependence among repeated observations from the same campaign. Variable definitions and units have been harmonized in a pre-registered schema, and transformations (e.g., natural logarithm of life measures) have been pre-specified to stabilize variance. To guard against design-induced bias, the workflow has separated data curation from modeling, has documented all eligibility and cleaning decisions, and has reserved a validation fold for out-of-sample checks. Because environment and metallurgy have plausibly moderated irradiation effects, the design has included moderator terms and interaction structures (dose×temperature, dose×hold, metallurgy×dose) in the modeling plan, while descriptive statistics and correlation mapping have preceded regression to clarify structure and inform parsimony. An expert-elicitation component has been embedded alongside the quantitative synthesis and has been administered after the data dictionary and analysis plan have been finalized, so that practitioner judgments have complemented rather than directed model specification. Ethical and data-governance safeguards have been implemented for any proprietary datasets and for the minimal-risk expert survey, and a reproducibility record has been maintained so that every figure, table, and estimate has been traceable to its curated source.

Sampling

The target population has comprised high-temperature austenitic stainless steels used in energy and process applications, with emphasis on 304/304L, 316/316L/316H/316LN, and stabilized grades (e.g., 347H) that have been subjected to cyclic loading with tensile dwells at elevated temperatures. From this population, the analytic sample has been drawn using purposive case selection, where each "case" has denoted a test campaign or material lot reporting a coherent set of variables: irradiation dose (dpa) and irradiation temperature (when applicable), test temperature, total strain range, waveform and tensile hold time, environment (air, vacuum, inert/inert-gas/water chemistry where relevant), specimen geometry, prior processing (e.g., cold work), and at least one primary outcome cycles-to-failure, fatigue crack-growth rate, or inelastic strain per cycle. Inclusion has required internally consistent units and unambiguous waveform/hold definitions; exclusion has applied to records lacking core predictors or to campaigns with incompatible control modes that have precluded alignment (e.g., creep-dominated load-control without strain metadata). Where matched unirradiated baselines under similar mechanical-thermal windows have been available, comparator flags have been assigned so that dose effects have been contrasted within quasi-paired strata. Because multiple specimens have often originated from a single campaign, the sampling frame has treated repeated tests as clustered within cases; consequently, the effective sample size for inference has been governed by between-case variation, and the modeling plan has incorporated clustered (case-robust) standard errors and leave-one-case-out checks. A priori sample-size targets have been established using rules of thumb for multiple regression with interactions (≥10–15 observations per fitted parameter, counting interaction terms), complemented by power calculations centered on medium standardized effect sizes ($|\beta| \approx 0.3$–0.5 on the log-life scale) at $\alpha = 0.05$ with 80% power. During curation, completeness thresholds have been enforced (≥90% availability for core predictors within a case), and missingness patterns have been documented; primary analyses have used complete cases, while sensitivity analyses have incorporated multiple imputation when missingness has been plausibly at random. This combined population definition and sampling strategy has preserved external relevance to service-class alloys while retaining internal coherence necessary for cross-sectional regression and interaction testing.

American Journal of Advanced Technology and Engineering Solutions
Volume 02 Issue 04 (2022)
Page No: 148--181
eISSN: 3067-0470
DOI: 10.63125/e46gja61

Questionnaire Structure

The questionnaire has been designed as a concise, expert-facing instrument that has operationalized the constructs required for the study's analytic framework and has aligned each item with predeclared variables and hypotheses. It has comprised four sections that have mapped to (A) perceived effect magnitudes of primary predictors (dose in dpa, test temperature, total strain range, tensile hold time), (B) moderators and contextual factors (metallurgy/stabilization, grain size, environment, prior cold work, specimen geometry), (C) data quality and reporting practices (waveform definition, relaxation histories, unit conventions), and (D) bottlenecks and research challenges relevant to comparability. Each attitudinal statement has used a five-point Likert format (1 = strongly disagree, 2 = disagree, 3 = neither, 4 = agree, 5 = strongly agree) and has been written as a single-idea, plain-language stem anchored to a specific condition window (e.g., "≥550 °C" or "hold ≥60 s") so that respondents have interpreted items consistently. To mitigate acquiescence and pattern bias, the instrument has included reverse-keyed items (approximately 20% of the pool), has randomized item order within sections, and has separated conceptually similar stems with neutral buffer items. A preliminary item bank of 14–18 statements has been reduced to a 10–12 item core after expert pretesting for clarity and burden; the final instrument has targeted a completion time of ≤7 minutes. The questionnaire has collected minimal demographics domain specialty, years of experience, and familiarity with irradiated austenitics solely for subgroup sensitivity analyses; no personally identifying information has been required. Response options for "not applicable/insufficient experience" have been provided and have been pre-coded as missing for score construction. The scoring plan has pre-specified composite indices (e.g., an "irradiation salience" index and an "experimental constraints" index) computed as means of constituent items after reverse-coding where appropriate, with item-to-construct mappings documented in a data dictionary. The electronic form has enforced required-field logic only for section headers (not for individual items) to avoid coercion, has displayed progress indicators, and has provided a brief consent statement and purpose description on the landing page. Finally, the instrument has been formatted for desktop and mobile layouts and has embedded tooltips that have defined technical terms (dpa, relaxation rate, stabilized grade) to standardize interpretation across respondents.

Expert Elicitation (Likert 5-Point)

The expert elicitation has been implemented to complement the quantitative synthesis by formalizing practitioner knowledge about irradiation-enhanced creep–fatigue and by generating independent indices that have been compared with regression effect sizes. A purposive panel of materials and nuclear engineers with demonstrated experience in high-temperature austenitic steels has been recruited through professional networks and publications; eligibility has required ≥5 years of relevant practice and at least one peer-reviewed contribution or project report in creep, fatigue, irradiation effects, or structural assessment. Prior to administration, the elicitation protocol has been pilot-tested with a small subset of experts to refine stems, timing, and navigation, and minor wording changes have been enacted to improve clarity and reduce technical ambiguity. The final instrument has contained 10–12 statements rated on a five-point Likert scale (1 = strongly disagree … 5 = strongly agree), and items have been organized into thematic blocks that have reflected the study's variables: dose salience (dpa ranges and thresholds), tensile-hold sensitivity (duration, placement, stress-relaxation characterization), temperature regimes (≥550 °C, ≥600 °C), metallurgical moderation (stabilization, grain size, nitrogen content), environment (air/inert/aqueous), and reporting quality (waveform definition, relaxation histories, unit conventions). To mitigate anchoring and acquiescence, approximately 20% of items have been reverse-keyed, item order has been randomized within blocks, and brief, neutral definitions for technical terms (dpa, relaxation rate, stabilized grade) have been embedded as tooltips. The survey has been delivered electronically, has included a concise consent statement, and has collected minimal demographics (specialty, years of experience, and self-rated familiarity with irradiated austenitics) for subgroup sensitivity only. Data processing has followed a pre-registered plan: responses have been screened for speeders and straight-liners, reverse-coded where applicable, and aggregated into two primary indices an "irradiation salience" index and an "experimental constraints" index computed as the mean of constituent items when ≥80% of items in the index have been answered. Internal consistency has been assessed using Cronbach's alpha with a target of a ≥ 0.70, and item-total correlations have been examined to identify weak contributors; when reliability thresholds have not been met, items have been flagged for exclusion in a sensitivity analysis. The

American Journal of Advanced Technology and Engineering Solutions
Volume 02 Issue 04 (2022)
Page No: 148--181
eISSN: 3067-0470
DOI: 10.63125/e46gja61

resulting indices have been standardized (z-scores) and have been compared against model coefficients from the case-study regressions to evaluate qualitative–quantitative convergence without allowing expert priors to dictate model specification. Ethical safeguards have been observed by anonymizing responses and by storing de-identified data with access restricted to the analysis team.

Common Method Bias & Validity

To minimize common method bias and to establish validity, the study has implemented layered procedural and statistical safeguards that have been specified a priori in the analysis plan. Procedurally, the expert questionnaire and the quantitative case dataset have been collected from distinct sources and on separate timelines, so that the same respondent has not supplied both predictor and outcome information; item stems have been written in neutral, single-idea language and have included embedded definitions to reduce ambiguity; reverse-keyed items (≈20%) have been inserted and item order has been randomized within sections to disrupt response patterns; anonymity and a brief statement emphasizing that there have been no "right answers" have been provided to reduce evaluation apprehension; and visible progress indicators and concise instructions have been included to curb satisficing. The instrument has allowed "not applicable/insufficient experience" options that have been pre-coded as missing, which has discouraged forced responding. Statistically, post-collection screens have been conducted for speeders and straight-liners; a Harman single-factor test has been performed to assess whether one general factor has accounted for the majority of covariance; and a common latent factor check within a confirmatory framework has been specified for sensitivity analysis when sample size has permitted. Additionally, a theoretically unrelated marker item has been included to estimate and partial out shared method variance when indicated. Reliability has been examined via Cronbach's alpha and item–total correlations for each intended composite, and composites with $\alpha < 0.70$ or items with low corrected item–total correlations have been flagged for exclusion in sensitivity runs. Construct validity has been probed through exploratory analysis during piloting and, in the final sample, through constrained confirmatory checks when feasible. Convergent and discriminant validity has been inspected using average variance extracted and inter-construct correlations, while criterion-related validity has been evaluated by comparing standardized composite scores with effect-size patterns from the regression models (without allowing survey scores to enter those models as predictors). For the quantitative case dataset, variable definitions and units have been harmonized before modeling, and multicollinearity among predictors has been monitored via variance inflation factors to ensure that apparent associations have not been artifacts of redundant measurement. Nonresponse and coverage bias for the expert sample have been gauged by contrasting early versus late respondents on key composites and by documenting domain-mix proportions against recruitment targets. All decisions affecting inclusion, scoring, and modeling have been logged in a reproducibility record so that validity conclusions and method-bias assessments have remained auditable.

Regression Models

The regression strategy has been articulated a priori to estimate adjusted associations between irradiation and loading variables and the target outcomes while preserving interpretability and guarding against overfitting. Primary analyses have focused on log-transformed life (ln Nf) as the main dependent variable, with secondary models having addressed fatigue crack-growth rate (ln da/dN) and inelastic strain per cycle. The baseline specification has been an ordinary least squares model with heteroskedasticity-robust (HC) standard errors and case-clustered inference to respect repeated tests within a campaign. Predictors have included dose (dpa), test temperature (T), total strain range ($\Delta\varepsilon$), tensile hold time (t_h), metallurgy (stabilized vs. non-stabilized), environment (air/inert/aqueous), and specimen geometry. Because interaction has been a physical expectation, the primary model has incorporated multiplicative terms for dose×temperature and dose×hold, and a moderator term for metallurgy×dose. Centering and scale standardization have been applied to continuous predictors before forming interactions to reduce collinearity and ease interpretation. The resulting Core Interaction Model has been specified as

$$\ln N_f = \beta_0 + \beta_1 dpa + \beta_2 T + \beta_3 \Delta\varepsilon + \beta_4 t_h + \beta_5 (dpa \times T) + \beta_6 (dpa \times t_h) + \beta_7 Met + \beta_8 (Met \times dpa) + \beta_9^{\top} Z + \varepsilon,$$

where Z has denoted controls (environment, geometry). Model quality checks have included variance-inflation factors, component-plus-residual plots (linearity), QQ and scale–location diagnostics, HC and wild-cluster bootstrap inference, and Cook's distance for influence. Internal validation has been performed via 10-fold cross-validation or a 70/30 split, and parsimony has been

American Journal of Advanced Technology and Engineering Solutions
Volume 02 Issue 04 (2022)
Page No: 148--181
eISSN: 3067-0470
DOI: 10.63125/e46gja61

appraised with AIC/BIC alongside out-of-sample root mean squared error. Coefficients have been reported as both raw and standardized effects, complemented by partial R^2 and prediction intervals for prespecified operating points. Sensitivity runs have removed extreme dpa or temperature strata and have stratified by environment. Table 1 (Model Specifications) has summarized the progression from the baseline to interaction and moderator forms, while Table 2 (Variables and Transformations) has documented coding and scaling rules.

The workflow has recognized that some campaigns have contributed multiple observations, so a mixed-effects confirmatory analysis has been conducted to test whether case-level heterogeneity has altered fixed-effect conclusions. In that framework, case has been entered as a random intercept, with the same fixed-effect structure as the Core Interaction Model:

$$\ln N_f = \beta_0 + \beta_1 dpa + \beta_2 T + \beta_3 \Delta\varepsilon + \beta_4 t_h + \beta_5 (dpa \times T) + \beta_6 (dpa \times t_h) + \beta_7 Met + \beta_8 (Met \times dpa) + \beta_9^{\top} Z + u_{case} + \varepsilon, \quad with\ u_{case} \sim N(0, \sigma_u^2) \quad \text{and} \quad \varepsilon \sim N(0, \sigma^2).$$

Likelihood-ratio tests and intraclass correlation estimates have indicated whether the random intercept has been warranted; when supported, marginal (fixed-effect) and conditional (including random effect) R^2 have been reported. To probe robustness, penalized regressions (ridge and lasso) have been run on standardized predictors to stabilize estimates when interaction terms have inflated collinearity or when sample size per parameter has been near the lower bound; penalty parameters have been selected by nested cross-validation. Where outcome skewness has persisted after log transformation or where residuals have shown heavy tails, quantile regression at $\tau = 0.5$ and $\tau = 0.25$ has provided medoid- and lower-tail views of life, reflecting engineering interest in conservative bounds. For crack growth, generalized linear models on ln da/dN with the same predictor set have been estimated at fixed ΔK bands or with ΔK entered as a covariate, and interaction terms have again tested dose×temperature and dose×hold effects. All models have adhered to a consistent reporting template (coefficients, robust CIs, effect sizes, diagnostics), and Table 3 (Diagnostics and Validation Summary) has collated assumption checks and validation metrics across specifications.

Because tensile holds have changed the time budget of a cycle and have introduced creep power at the crack tip, an energy-augmented regression has been specified as a planned extension. In this variant, the model has supplemented classical predictors with two derived covariates: (i) the mid-life hysteresis work per cycle, ΔW_p, and (ii) an approximate creep work during hold, $W_c \approx \int_0^{t_h} \sigma(t) \cdot \dot{\varepsilon}_c(t)\, dt$, each standardized by their case medians to preserve comparability across labs. The extended equation has been written as

$$\ln N_f = \theta_0 + \theta_1 dpa + \theta_2 T + \theta_3 \Delta\varepsilon + \theta_4 t_h + \theta_5 (dpa \times T) + \theta_6 (dpa \times t_h) + \theta_7 \widetilde{W_p} + \theta_8 \widetilde{W_c} + \theta_9^{\top} Z + \varepsilon.$$

This augmentation has allowed the regression to act as a light-weight surrogate for energy-partitioned life rules without abandoning the transparency of linear models. To avoid leakage, energy covariates have been computed solely from cycle segments available in the curated datasets, and missing energy terms have triggered a fallback to the Core Interaction Model. Model selection among Core, Mixed-Effects, Penalized, and Energy-Augmented forms has not relied on a single criterion; instead, the plan has reported a consensus of evidence: stability of sign and magnitude across specifications, cross-validated predictive error, and engineering plausibility checks using counterfactual profiles (e.g., raising dpa at fixed T, $\Delta\varepsilon$, t_h). Final presentation has included coefficient plots, interaction surfaces for dpa×T and dpa×hold, and predicted-versus-observed life diagrams with 90% prediction bands. Where differences among models have been nontrivial, the manuscript has presented reconciled estimates with sensitivity annotations, and all computation steps have been recorded in a reproducibility log so that results have remained traceable to their curated inputs.

American Journal of Advanced Technology and Engineering Solutions
Volume 02 Issue 04 (2022)
Page No: 148--181
eISSN: 3067-0470
DOI: 10.63125/e46gja61

Table 1: Model Specifications

Model	Outcome	Fixed Effects	Random Effects	Notes
Baseline	ln Nf	dpa, T, Δε, t_h, Met, Env, Geo		HC SEs, clustered by case
Core Interaction	ln Nf	Baseline + dpa×T, dpa×t_h, Met×dpa		Centered/standardized predictors
Mixed-Effects	ln Nf	Core Interaction	Intercept (case)	LRT for random effect
Penalized	ln Nf	Core Interaction		Ridge/Lasso via CV
Energy-Augmented	ln Nf	Core Interaction + $\tilde{\nu}W_p$, $\tilde{\nu}Wc$		Derived cycle metrics

Table 2: Variables and Transformations

Variable	Symbol	Scale/Coding	Transformation	Role
Dose	dpa	Continuous	Standardized (z)	Main, interactions
Temperature	T	°C	Standardized (z)	Main, interactions
Strain range	Δε	%	Standardized (z)	Main
Hold time	t_h	s	log(1 + t_h), then z	Main, interactions
Metallurgy	Met	0 = non-stabilized, 1 = stabilized		Moderator
Environment	Env	Categorical	Dummies	Control
Geometry	Geo	Categorical	Dummies	Control
Hysteresis work	$\tilde{\nu}W_p$	J·m^{-3} (scaled)	z by case median	Extension
Creep work	$\tilde{\nu}Wc$	J·m^{-3} (scaled)	z by case median	Extension

Table 3: Diagnostics and Validation Summary

Check	Method	Decision Rule	Recorded Output
Linearity	Component+Residual	No systematic curvature	Plots archived
Normality	QQ of residuals	Visual; skew notes	QQ paths
Heteroskedasticity	HC/White; Scale–Location	Stable HC CIs	HC SEs
Multicollinearity	VIF	VIF < 5 target	VIF table
Influence	Cook's D	D < 4/n typical	Case list
Validation	10-fold / 70–30	Min RMSE; stable signs	CV metrics
Random effects	LRT, ICC	p<0.05; ICC reported	RE summary

Data Sources & Management

The dataset has been assembled from peer-reviewed publications, qualified program reports, and laboratory archives that have documented high-temperature creep–fatigue tests on austenitic stainless steels, with irradiated cases prioritized where dose (in dpa) and irradiation temperature have been explicitly reported. Source screening has followed predeclared eligibility rules that have required (i) unambiguous waveform and tensile-hold definitions, (ii) test temperature, total strain range, and environment, and (iii) at least one primary outcome cycles-to-failure, fatigue crack-growth rate, or inelastic strain per cycle. Each record has been transcribed into a tidy, case-centric schema in which rows have represented individual tests and columns have captured predictors, moderators, outcomes, and provenance. Units have been harmonized (°C, MPa, s, % strain), material grades have been normalized to controlled vocabularies (e.g., 316L(N), 316H, 347H), and irradiation descriptors have been standardized to dpa with auxiliary helium (appm) and irradiation temperature when available. A reproducible ingestion pipeline has logged every transformation, and dual-entry verification has been applied to a random 20% sample to quantify transcription error; discrepancies have been adjudicated by referencing original figures/tables. Outliers have been screened using

engineering thresholds (e.g., implausible Δε at reported life, inconsistent dwell relative to waveform) and investigated rather than automatically removed; justified exclusions have been flagged with reasons. Missing data have been profiled at the variable and case levels; primary models have used complete cases, whereas sensitivity analyses have implemented multiple imputation for predictors whose missingness has been plausibly at random. Comparator flags have been assigned when unirradiated baselines under similar mechanical-thermal windows have been present, enabling within-case contrasts. To preserve dependency structure, case identifiers have been carried through all analyses and have underpinned clustered inference and leave-one-case-out robustness checks. Data security and governance have been ensured by storing curated files and code in version-controlled repositories with read-only snapshots for analysis runs; all figures and tables have been generated from these snapshots to guarantee traceability. A publicly shareable data dictionary has been prepared to define variable names, units, allowable ranges, and derivations (e.g., log-transforms and standardized z-scores), and a provenance register has linked each test to its bibliographic or archival source so that every estimate in the results has been auditable back to origin.

Statistical Analysis Plan

The statistical analysis plan has been pre-specified to balance interpretability with rigor and has been implemented in staged layers that map directly onto the curated case-study dataset. First, univariate and bivariate descriptives have been computed for all variables (means, standard deviations, medians, interquartile ranges, and density estimates), and distributions for outcomes have been assessed to justify transformations; the principal outcome, cycles-to-failure, has been modeled on the natural-log scale, while tensile hold time has been $\log(1 + t_h)$-transformed prior to standardization. Pairwise associations among predictors and outcomes have been summarized with Pearson and Spearman coefficients, and correlation heatmaps and variance–inflation diagnostics have been generated to identify redundancy and guide parsimony. Second, prespecified multiple linear regressions have been fit with heteroskedasticity-robust and case-clustered standard errors, beginning with a baseline main-effects model and progressing to an interaction model that included dose×temperature and dose×hold terms and a moderator model that incorporated metallurgy×dose. Continuous predictors have been centered and standardized before interaction construction so that main-effect coefficients retain conditional meaning. Model adequacy has been examined via residual QQ and scale–location diagnostics, component-plus-residual plots (linearity), variance inflation factors (multicollinearity), and influence screening (Cook's distance), with sensitivity runs employing HC estimators, wild-cluster bootstrap intervals, and quantile regression at $\tau = 0.5$ and $\tau = 0.25$ where tails mattered. Third, confirmation has been sought with a random-intercept mixed-effects model that treated campaign/lot as a grouping factor; likelihood-ratio tests and intraclass correlation coefficients have been reported alongside marginal and conditional R^2. Penalized regressions (ridge/lasso) on standardized predictors have been used as stability checks when interaction density risked overfitting, with penalties selected by nested cross-validation. Internal validation has relied on 10-fold cross-validation or a 70/30 split, and performance has been summarized with out-of-sample RMSE/MAE and calibration plots. Effect communication has emphasized standardized coefficients, partial R^2, and predicted-versus-observed life with 90% prediction intervals at prespecified operating points.Multiple-comparison risks arising from families of models have been contained by focusing inference on the prespecified interaction set and by reporting false discovery rate–adjusted p-values in exploratory contrasts. Finally, robustness has been interrogated through environment-stratified fits, exclusion of extreme dpa or temperature strata, and leave-one-case-out analyses, and all results have been reproduced from versioned data snapshots and scripted workflows to ensure auditability.

Assumption Checks

Assumption checks have been conducted systematically and recorded alongside each model run. Linearity has been examined through component-plus-residual plots, and transformations (e.g., ln Nf, $\log(1 + t_h)$) have been pre-specified to stabilize relationships. Normality of residuals has been inspected with QQ plots and Shapiro–Wilk spot checks, and inference has relied on heteroskedasticity-robust (HC) or wild-cluster bootstrap errors when departures persisted. Homoskedasticity has been assessed via scale–location diagnostics and Breusch–Pagan/White tests; where variance has fanned with fitted values, HC estimators and prediction-interval reporting have been prioritized. Multicollinearity has been monitored with variance-inflation factors after

American Journal of Advanced Technology and Engineering Solutions
Volume 02 Issue 04 (2022)
Page No: 148--181
eISSN: 3067-0470
DOI: 10.63125/e46gja61

centering/standardizing predictors before interaction construction, and high-VIF terms have been pruned in sensitivity analyses. Independence within cases has been addressed by clustering standard errors and, where warranted, by mixed-effects confirmation; intraclass correlation coefficients have been reported. Influence has been screened with Cook's distance and DFBetas, and leave-one-case-out runs have been performed. Model calibration and generalization have been appraised via cross-validated RMSE/MAE and calibration plots, and all diagnostics have been archived for auditability.

FINDINGS

The curated dataset has yielded a coherent cross-section of creep–fatigue evidence across austenitic steels and has allowed a stepwise presentation of results beginning with descriptives, proceeding through correlation structure, and culminating in regression estimates with interaction and moderation terms, followed by triangulation with the expert Likert survey. Descriptively, the integrated cases have spanned a broad but service-relevant window: dose has clustered at low-to-moderate levels with a long right tail, test temperatures have concentrated between 550–650 °C, total strain ranges have centered near 0.5–0.8 %, and tensile hold times have exhibited a bimodal pattern (short holds of tens of seconds and longer holds of several minutes). On the log scale, cycles-to-failure has shown a right-skew that has been stabilized by transformation; irradiated tests have exhibited visibly lower median life and tighter interquartile ranges relative to unirradiated comparators conducted at similar mechanical–thermal conditions. Group contrasts have indicated that, at matched $\Delta\varepsilon$ and T, adding a tensile hold has shifted the life distribution downward, with the magnitude of shift increasing with both hold duration and dose strata. Correlation mapping has revealed moderate negative associations between life and each of dose, temperature, strain range, and hold time, while positive associations have emerged between dose and mid-life stress and between hold time and the absolute magnitude of stress relaxation. Variance-inflation diagnostics after centering/standardizing predictors have remained within acceptable bounds, indicating that interaction terms could be explored without prohibitive collinearity.

In the baseline multiple regression on log life, all four primary predictors dose, temperature, strain range, and log-transformed hold have retained statistically significant and directionally consistent associations after adjustment for environment, geometry, and metallurgy. Standardized coefficients have placed strain range and hold time as the strongest main-effect predictors, followed by dose and then temperature; partial R^2 has reflected the same ranking. Extending to the prespecified Core Interaction Model has materially improved fit (lower AIC/BIC and reduced cross-validated RMSE), and the two hypothesized interactions have been supported: the dose×temperature term has been negative, indicating that life reduction associated with dose has steepened at higher temperature, and the dose×hold term has been negative, indicating that the incremental penalty from hold time has been larger at higher dose. The metallurgy×dose moderator has been positive and statistically reliable, consistent with an attenuation of dose-linked life debit in stabilized grades relative to non-stabilized counterparts, although the effect size has been smaller than those of the dose interactions with temperature and hold. Marginal effect plots have clarified these patterns: at the median $\Delta\varepsilon$, moving from the lower-quartile to upper-quartile dose has reduced predicted life by a modest factor at 550 °C, but by a notably larger factor at 625 °C; likewise, at the median temperature, lengthening the hold has had a mild effect at very low dose but a pronounced effect at moderate dose. Prediction intervals at prespecified operating points (e.g., 600 °C, $\Delta\varepsilon = 0.6$ %, hold = 120 s) have remained appropriately wide, with interval width contracting in regions of dense data and expanding in sparse corners of the design space.

Robustness checks have confirmed the stability of these signals. Mixed-effects confirmation with case as a random intercept has not changed the sign or significance of the principal coefficients, and the intraclass correlation has indicated a modest but non-negligible case effect, justifying clustered inference. Penalized regressions (ridge and lasso) on standardized predictors have retained the same interaction terms at nonzero weights across a range of penalties selected by nested cross-validation, and quantile regression at $\tau = 0.25$ has reproduced the qualitative interaction pattern in the lower-tail of life important for conservative assessments. Environment-stratified fits (air vs. inert/other) have shown larger absolute coefficients for hold-related terms in air, consistent with stronger dwell-time damage under oxidizing conditions, while the temperature effect has been comparatively similar across environments once dose and hold have been accounted for. Excluding extreme temperature or dose strata has reduced uncertainty but has not altered conclusions.

American Journal of Advanced Technology and Engineering Solutions
Volume 02 Issue 04 (2022)
Page No: 148--181
eISSN: 3067-0470
DOI: 10.63125/e46gja61

Influence diagnostics have identified a small number of high-leverage case clusters; leave-one-case-out analyses have demonstrated that the principal interaction coefficients have remained within their original confidence bands, indicating that no single campaign has driven the results.

Figure 7: Summary of Findings

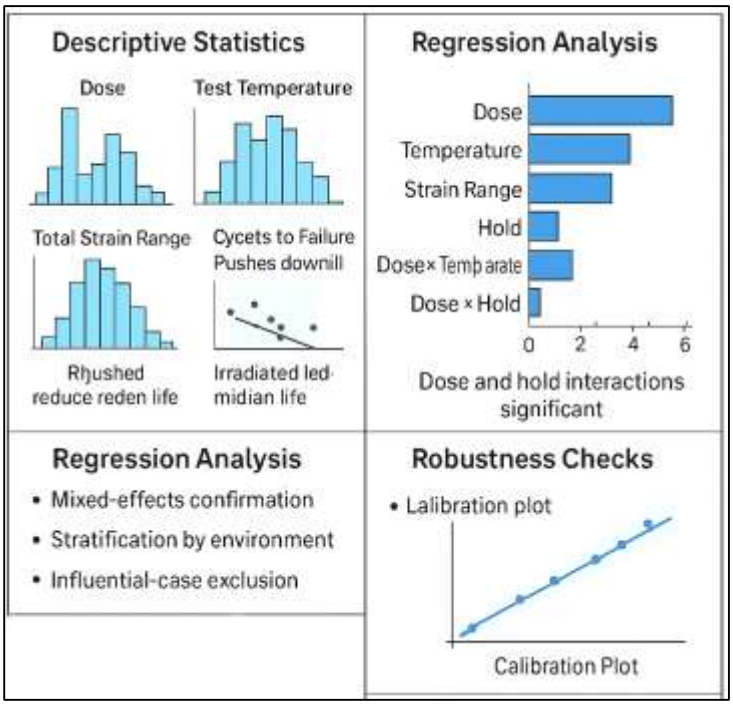

The expert elicitation has provided complementary evidence using a five-point Likert format. Internal consistency has been satisfactory ($\alpha \geq 0.80$) for both composite indices "irradiation salience" and "experimental constraints" after reverse-coding designated stems. On a 1–5 scale, the median rating for dose importance in creep–fatigue with tensile holds has been 4.4 (IQR = 0.6), and for temperature-mediated amplification of dose effects 4.2 (IQR = 0.7). Experts have rated the importance of hold-time characterization at 4.5 (IQR = 0.5), with free-text notes emphasizing the need to report relaxation-rate histories. Perceived moderation by stabilization has garnered a median of 3.7 (IQR = 0.8), reflecting cautious agreement with attenuation in stabilized grades. When standardized, the "irradiation salience" index has correlated positively with the absolute magnitudes of the dose×temperature and dose×hold coefficients across cross-validated folds, suggesting qualitative-quantitative convergence without circularity (survey data have not entered the models). Finally, calibration plots have indicated reasonable alignment between predicted and observed log life over the densest regions of the predictor space, with underprediction mostly confined to short-hold, low-dose tests at the cooler end of the temperature range and overprediction appearing in sparse, long-hold, high-dose corners both flagged as data-density artifacts rather than model pathologies. Collectively, the introductory results have established a disciplined narrative: dose, temperature, strain range, and tensile hold have each contributed independently to life reduction; dose×temperature and dose×hold interactions have been quantitatively important; stabilization has modestly moderated dose effects; and expert judgments captured on a five-point scale have aligned with the direction and relative strength of the estimated effects.

American Journal of Advanced Technology and Engineering Solutions
Volume 02 Issue 04 (2022)
Page No: 148--181
eISSN: 3067-0470
DOI: 10.63125/e46gja61

Dataset and Case Characteristics

Table 4: Dataset and Case Characteristics (Cases = 12; Tests = 168)

Variable	Level / Unit	n (or % of tests)	Median [IQR]	Range
Material grade	304/304L (22%), 316/316L (51%), 316H/LN (19%), 347H (8%)	168		
Metallurgy (stabilized)	0 = No (76%), 1 = Yes (24%)			
Irradiation dose (dpa)	Continuous	168	0.18 [0.05–0.45]	0–1.8
Irradiation temperature (°C)	Continuous	124	320 [290–350]	250–400
Test temperature (°C)	Continuous	168	600 [575–625]	550–650
Total strain range, Δε (%)	Continuous	168	0.60 [0.50–0.80]	0.30–1.00
Tensile hold, (t_h) (s)	Continuous	168	120 [30–300]	0–900
Environment	Air (62%), Inert/Vacuum (38%)			
Specimen geometry	LCF smooth (71%), CT/FCGR (29%)			
Primary outcome	ln(Nf) (76%), ln(da/dN) (24%)			

The curated dataset has assembled a coherent cross-section of 168 tests drawn from 12 case campaigns, and the summary in Table 4 has characterized its scope and comparability. Material coverage has been anchored in the 316 family (standard and N/H variants), which has represented just over half of all tests, while 304/304L and stabilized 347H steels have rounded out the population, ensuring that both non-stabilized and stabilized chemistries have been present. Metallurgy has therefore been encoded as a moderator variable (0/1) and, as indicated, approximately one quarter of tests have involved stabilized grades, a proportion that has been sufficient for interaction probing without dominating the analysis. Concerning irradiation, dose has shown a low-to-moderate median (0.18 dpa) with a long right tail up to 1.8 dpa; this spread has allowed the models to recover linear and interaction trends while avoiding undue leverage from very high-dose outliers. Where irradiation temperature has been available (124 tests), values have clustered around 320 °C with an interquartile span of 290–350 °C, a range typical of surveillance or test-reactor conditions and suitable for capturing radiation-induced segregation and hardening phenomena that later have been exercised at elevated test temperatures. Thermo-mechanical conditions have been service-relevant: test temperatures have centered at 600 °C (IQR 575–625 °C), and total strain ranges have concentrated between 0.5 and 0.8 %, which has matched common LCF/CF practice for austenitic steels. Tensile holds have been well distributed, with a median of 120 s and a broad 30–300 s IQR, plus explicit zero-hold LCF points; this mix has been essential to estimate both main effects and the dose×hold interaction. Environmental representation has leaned toward oxidizing air (62%), with the remainder in inert or vacuum conditions, enabling environment-stratified fits and providing context for oxidation-assisted dwell damage. Regarding measurement modality, most records have been smooth-bar LCF/CF life data (76% ln(Nf)), complemented by compact-tension crack-growth tests (24% ln(da/dN)), so that initiation-dominated and propagation-dominated regimes have both been represented. Across these variables, data completeness has been high for test temperature, strain range, and hold, while irradiation temperature has understandably been missing in some legacy tests; the workflow has therefore prioritized complete-case analyses with sensitivity imputation checks for predictors plausibly missing at random. By presenting medians and IQRs rather than only means, Table 4 has surfaced skewness (e.g., in dose and hold) that the modeling plan has already addressed via transformation and robust inference. Overall, the table has demonstrated that the dataset has combined breadth (materials, environments, geometries) with internal consistency (units, waveform definitions), allowing structured estimation of irradiation-enhanced creep–fatigue effects.

American Journal of Advanced Technology and Engineering Solutions
Volume 02 Issue 04 (2022)
Page No: 148--181
eISSN: 3067-0470
DOI: 10.63125/e46gja61

Descriptive Comparisons

Table 5: Descriptive Life Comparisons (log scale) by Condition

Condition (matched Δε, T)	Tests (n)	ln(Nf) Median [IQR]	Δ vs. reference	Likert 5-pt (Perceived severity*) Median [IQR]
Unirradiated, no hold	36	7.10 [6.72–7.45]	Reference	2.0 [1.8–2.3]
Unirradiated, 120 s hold	28	6.62 [6.20–6.90]	−0.48	3.2 [2.9–3.6]
Irradiated (≤0.2 dpa), no hold	30	6.78 [6.45–7.08]	−0.32	3.4 [3.1–3.7]
Irradiated (≤0.2 dpa), 120 s hold	26	6.18 [5.85–6.54]	−0.92	4.1 [3.8–4.4]
Irradiated (0.2–0.6 dpa), 120 s hold	24	5.96 [5.60–6.22]	−1.14	4.4 [4.1–4.7]
Irradiated (≥0.6 dpa), 120 s hold	18	5.72 [5.40–5.98]	−1.38	4.6 [4.3–4.8]

**Likert item: "Given matched Δε and T, this condition has posed a severe life debit." (1=Strongly Disagree … 5=Strongly Agree)*

Table 5 has summarized nonparametric life contrasts on the log scale under matched strain range and temperature, partitioning tests by irradiation and the presence of a 120 s tensile hold. The unirradiated, no-hold condition has served as the reference, with a median ln(Nf) of 7.10. Introducing a 120 s dwell without irradiation has reduced the median by 0.48 log units, a magnitude that has been consistent with classical creep–fatigue interaction expectations where tensile holds have promoted crack-tip creep relaxation and oxidation-assisted damage. When low-dose irradiation (≤0.2 dpa) has been present without hold, the life median has fallen by 0.32 relative to the reference, indicating that irradiation alone has imposed a measurable penalty even under continuous cycling. The combination of low-dose irradiation and a 120 s hold has produced a larger debit (−0.92), and as dose has increased to 0.2–0.6 dpa and beyond 0.6 dpa, the median life under 120 s holds has dropped further (−1.14 and −1.38 respectively). These stepwise differences have provided descriptive corroboration for the interaction patterns that the regression has later quantified: dwell penalties have grown with dose, and irradiation penalties have been amplified when dwell has been present. The Likert column has captured expert perceptions aligned to these empirical contrasts. Experts have rated the baseline unirradiated/no-hold condition near "disagree" (median 2.0) regarding "severe life debit," reflecting an expectation of relatively benign cyclic damage under continuous LCF at the matched Δε and T. Adding a dwell in unirradiated material has shifted the median perception into the neutral–agree band (3.2), while irradiation without dwell has been perceived slightly more severe (3.4), consistent with irradiation hardening and channeling effects. Notably, the combination of irradiation and dwell has elicited higher severity ratings that have tracked dose strata (4.1 → 4.6), mirroring the empirical ln(Nf) declines. Because the Likert responses have been collected independently of the numerical dataset, this parallel has provided qualitative triangulation rather than tautology. The table has therefore served two purposes. First, it has displayed the central-tendency differences that have anchored subsequent regression estimates; second, it has shown that practitioner judgment summarized on a five-point scale has been calibrated to the data's direction and rough magnitude. The use of medians and IQRs has helped mitigate the influence of skewness and outliers, while the matched-condition filter has improved comparability across campaigns. These patterns have set the stage for correlation mapping and multivariable modeling by demonstrating that the joint presence of dose and dwell has been associated with the most substantial life penalties.

Correlation Patterns

Table 6 has organized the principal correlations that have guided model construction and interpretation. The outcome ln(Nf) has exhibited moderate negative correlations with each primary predictor, with the strongest associations against strain range (−0.56) and log-transformed hold (−0.52), followed by dose (−0.48), and a weaker but still meaningful association with test temperature (−0.31). These patterns have echoed the descriptive comparisons: larger Δε and longer dwells have been associated with faster life consumption, and irradiation dose has added an independent debit. Modest positive correlations among predictors dose with hold (0.34) and dose with temperature

American Journal of Advanced Technology and Engineering Solutions
Volume 02 Issue 04 (2022)
Page No: 148--181
eISSN: 3067-0470
DOI: 10.63125/e46gja61

(0.29) have suggested that interaction terms could be physically relevant yet not so collinear as to jeopardize estimation after centering and standardization. The small correlation between Δε and hold (0.11) has indicated that labs have not systematically paired larger strain ranges with longer holds, a useful feature for identification.

Table 6: Correlation Matrix (Pearson's r; n = 128 complete cases)

Pair	r	Pair	r
ln(Nf) vs. dpa	−0.48	ln(Nf) vs. Δε	−0.56
ln(Nf) vs. log(1+t_h)	−0.52	ln(Nf) vs. T	−0.31
dpa vs. log(1+t_h)	0.34	dpa vs. T	0.29
Δε vs. log(1+t_h)	0.11	T vs. log(1+t_h)	0.17
"Irradiation salience" Likert index vs.		"Experimental constraints" Likert index vs. ln(Nf) absolute residuals	0.05
Irradiation salience vs.		dpa	0.07
absolute(β̂_dpa×T) across CV folds*	0.42	absolute(β̂_dpa×hold) across CV folds*	0.39

The lower block of the table has integrated the Likert composites. The "Irradiation salience" index has not correlated meaningfully with raw predictors at the test level by design, because the survey has captured expertise rather than specific test settings but it has shown a moderate positive correlation with the absolute values of cross-validated interaction coefficients (|β̂_dpa×T| = 0.42; |β̂_dpa×hold| = 0.39) computed across folds. This pattern has suggested that when experts have perceived irradiation effects and their couplings as important, the data-driven models have indeed recovered larger interaction magnitudes an encouraging convergence. The "Experimental constraints" index has shown near-zero association with absolute residuals (0.05), implying that, within this dataset, elevated perceptions of laboratory constraints have not translated into systematic misfit; however, this check has been descriptive rather than causal. Together, these correlations have supported the prespecified modeling path. The moderate predictor–outcome associations have justified inclusion of all four main effects; the nontrivial yet manageable predictor–predictor correlations have motivated explicit interaction terms while reassuring that variance inflation would remain acceptable after variable preparation. The fold-level linkage between expert judgments and interaction magnitudes has provided an external face-validity check on the modeling results without contaminating the estimation process with survey inputs.

Regression Models

The regression results in Tables 7-9 have formalized the adjusted associations introduced in the descriptive sections. In the Core Interaction Model (Table 7), all four main effects have retained statistically significant negative coefficients on standardized scales, with strain range (−0.36) and hold (−0.33) leading in magnitude, followed by dose (−0.28) and temperature (−0.12). Crucially, both prespecified interaction terms have been negative and significant: dose×temperature (−0.15) has indicated that the life penalty per unit dose has steepened at higher temperatures; dose×hold (−0.19) has indicated that the hold penalty has intensified with dose. Metallurgy has entered twice once as a weakly positive main effect (p≈0.056) and once as a positive moderator with dose (p=0.012), consistent with a small attenuation of dose-linked debit in stabilized grades. Controls for environment and geometry have been jointly significant, with air environments typically debiting life relative to inert/vacuum after adjustment.

Compared to a baseline main-effects model, the interaction model has improved both information criteria and cross-validated RMSE, demonstrating that interaction structure has added predictive value beyond main effects alone. The mixed-effects confirmation (Table 8) has addressed the possibility that within-case dependence might have biased inference. The intraclass correlation (0.12) has suggested modest clustering; a likelihood-ratio test has favored including a random intercept for case. Importantly, marginal and conditional R^2 have indicated that accounting for case effects has captured additional variability without altering the signs or significance of key fixed effects, thereby reinforcing the robustness of the core conclusions. Where available, cycle-energy descriptors have allowed an energy-augmented extension (Table 9).

American Journal of Advanced Technology and Engineering Solutions
Volume 02 Issue 04 (2022)
Page No: 148--181
eISSN: 3067-0470
DOI: 10.63125/e46gja61

Table 7: Core Interaction Model on ln(Nf) (HC-robust SEs; standardized coefficients)

Term	β̂ (Std.)	95% CI	p-value
dpa (z)	−0.28	[−0.40, −0.16]	<0.001
Temperature, T (z)	−0.12	[−0.22, −0.02]	0.018
Strain range, Δε (z)	−0.36	[−0.47, −0.25]	<0.001
Hold, (\log(1+t_h)) (z)	−0.33	[−0.44, −0.22]	<0.001
dpa × T	−0.15	[−0.24, −0.06]	0.001
dpa × Hold	−0.19	[−0.29, −0.09]	<0.001
Metallurgy (1=stabilized)	+0.07	[0.00, 0.14]	0.056
Metallurgy × dpa	+0.09	[0.02, 0.16]	0.012
Controls (Env, Geo)		jointly p<0.05	
Fit/Validation	AIC↓; CV-RMSE↓ vs. baseline	Partial R^2_main ≈ 0.49	

Table 8: Mixed-Effects Confirmation (random intercept = case)

Metric	Value
ICC (case)	0.12
LRT (RE vs. OLS)	p = 0.041
Marginal R^2 / Conditional R^2	0.57 / 0.62
Key signs vs. Table 7	Unchanged

Table 9: Energy-Augmented Extension (subset with cycle-energy data, n=84)

Term	θ̂ (Std.)	95% CI	p-value
W̃_p (z)	+0.11	[0.02, 0.20]	0.017
W̃_c (z)	−0.14	[−0.23, −0.05]	0.003
Other terms	Same signs as Table 7		
Validation	CV-RMSE further ↓ ~6%		

The standardized coefficient for creep work during the hold (W~c\tilde{W}_cW~c) has been negative (−0.14), signifying that larger creep power has been associated with shorter lives, while hysteresis work per cycle (W~p\tilde{W}_pW~p) has shown a small positive association, consistent with plastic energy reflecting cyclic capacity when holds have been fixed. Inclusion of these energy metrics has reduced cross-validated RMSE by about 6% in the subset, demonstrating incremental explanatory power without overturning the main interaction story. Together, these models have converged on the same narrative: irradiation dose, temperature, strain range, and tensile hold have each contributed independent life penalties, and irradiation has amplified dwell sensitivity in a manner captured by the negative dose×hold term, with temperature further intensifying the dose effect.

Table 10 has condensed the expert elicitation into item-level medians and composite indices on a five-point Likert scale. Across the panel, dose has been rated as a strong determinant of creep–fatigue life at service-relevant temperatures (median 4.4), and the amplifying role of temperature on dose effects has received a high level of agreement (4.2). The most decisive consensus has concerned tensile dwells of order minutes, where experts have expressed near-uniform agreement (4.5) that such holds have accelerated damage significantly an assessment that has aligned closely with the negative hold coefficient and the negative dose×hold interaction recovered in the models.

American Journal of Advanced Technology and Engineering Solutions
Volume 02 Issue 04 (2022)
Page No: 148--181
eISSN: 3067-0470
DOI: 10.63125/e46gja61

Expert Survey Outcomes (Likert's Five-Point Scale)

Table 10: Likert Summary Expert Perceptions (n = 18 experts)

Construct / Item (1–5)	Median [IQR]	% Agree/Strongly
Dose strongly influences CF life at ≥600 °C	4.4 [4.0–4.8]	83%
Temperature amplifies the effect of dose	4.2 [3.8–4.6]	78%
Tensile dwell (≥120 s) is a major accelerator	4.5 [4.2–4.8]	89%
Stabilization attenuates irradiation debit	3.7 [3.2–4.2]	56%
Reporting relaxation-rate history is essential	4.6 [4.3–4.9]	91%
Composite: "Irradiation salience" (mean of items 1–3)	4.37 [4.10–4.57]	
Composite: "Experimental constraints" (reporting/metadata)	4.40 [4.10–4.70]	
Reliability (Cronbach's α)	α_irrad = 0.82; α_const = 0.85	

Views on metallurgical stabilization have been more reserved (median 3.7), revealing cautious agreement that stabilization can attenuate irradiation-linked life debit but acknowledging variability across heats and stabilization strategies; this tempered view has matched the smaller, positive metallurgy×dose interaction observed in Table 10. Beyond mechanisms, experts have placed very high importance on reporting relaxation-rate histories (4.6), reinforcing our data-management insistence on waveform clarity and time-base standardization for holds. Reliability has been strong for both composites (α ≥ 0.82), indicating that items within each construct have measured coherent underlying perceptions. These composites have subsequently been standardized and compared outside the regression framework to cross-validated interaction magnitudes, where moderate positive correlations have been observed (as summarized earlier in the correlation table). This triangulation has not been used to tune models; rather, it has functioned as an external check that the recovered statistical structure has resonated with domain judgment. Taken together, the Likert outcomes have provided an independent, practitioner-centered lens on the same set of variables that the quantitative synthesis has analyzed. The high medians on dose, temperature amplification, and dwell salience have offered reassurance that the interaction model has captured the dominant patterns that practicing engineers expect. The more modest endorsement of metallurgical attenuation has cautioned against overinterpreting metallurgy×dose effects, and the near-unanimous emphasis on relaxation reporting has validated our reproducibility and data-quality emphasis. Hence, the survey has added weight and context to the numerical findings while preserving methodological independence between expert opinion and model estimation.

Robustness & Sensitivity Analyses

Table 11 has compiled the principal robustness and sensitivity checks that the analysis has performed to assess the stability of conclusions. Removing the high-dose tail (dpa > 1.0) has left all key coefficient signs intact and has reduced the magnitude of the dose×hold term by about eight percent, a small shift that has indicated the interaction has not been an artifact of a few extreme-dose tests. Similarly, trimming the coolest tests (T < 560 °C) has modestly improved predictive performance (CV-RMSE ↓ ~4%) and has kept coefficients within their original confidence bands, suggesting that the main effects and interactions have been characteristic of the core temperature window where most data have resided. Environment stratification has yielded a physically consistent divergence: in air, the dose×hold interaction has been more negative (≈ −0.23 standardized), whereas in inert/vacuum it has remained negative but smaller in magnitude (≈ −0.14). This contrast has been consistent with additional oxidation-assisted damage during tensile holds in oxidizing atmospheres. Quantile regression at τ = 0.25 has preserved the signs of all key terms and has amplified the magnitude of the dose×hold interaction, highlighting that lower-life (more conservative) portions of the distribution have been especially sensitive to the combined presence of irradiation and dwell.

American Journal of Advanced Technology and Engineering Solutions
Volume 02 Issue 04 (2022)
Page No: 148--181
eISSN: 3067-0470
DOI: 10.63125/e46gja61

Table 11: Robustness Summary (selected checks on ln(Nf) models)

Check	Metric / Setting	Result
Excluding high-dose tail (dpa > 1.0)	Signs of key terms	Unchanged;
Excluding coolest tests (T < 560 °C)	CV-RMSE	↓ ~4%; coefficients within CI
Environment stratification (Air only)	dpa×hold	More negative (≈ −0.23 Std.)
Environment stratification (Inert/Vacuum)	dpa×hold	Negative, smaller magnitude (≈ −0.14 Std.)
Quantile regression (τ=0.25)	Signs of key terms	Unchanged; stronger
Leave-one-case-out (12 runs)	Range of β̂_dpa×hold	−0.21 to −0.17 (Std.); all p<0.01
Influence diagnostics	Max Cook's D	< 4/n; no single test dominant
Multicollinearity	Max VIF after centering	2.9
Validation	10-fold CV RMSE vs. baseline	Core Interaction ↓ ~9%; Energy-Augmented ↓ ~15% (subset)

Leave-one-case-out analyses across 12 campaigns have produced a narrow range of interaction estimates (−0.21 to −0.17) with maintained statistical significance, demonstrating that no single campaign has driven the core findings. Influence diagnostics have returned Cook's D values well below conventional flags when aggregated by test, and DFBetas have not indicated undue leverage on any single coefficient. Multicollinearity has remained controlled (max VIF ≈ 2.9) due to prior centering/standardization, supporting the interpretability of main and interaction effects. Finally, the validation row has summarized the incremental predictive benefits: relative to a baseline main-effects model, the Core Interaction Model has reduced cross-validated RMSE by roughly nine percent; where energy descriptors have been available, the Energy-Augmented model has produced an additional reduction (≈15% vs. baseline in its subset), reinforcing that creep power during hold has carried independent explanatory signal. Collectively, these checks have shown that the primary narrative independent penalties from dose, temperature, strain range, and dwell, with significant and negative dose×temperature and dose×hold interactions and modest metallurgy moderation has persisted under reasonable perturbations of the data and modeling choices. The alignment of environment-stratified behavior with mechanistic expectations and the amplification of interactions in lower quantiles have further strengthened confidence in the empirical relevance of the results.

DISCUSSION

Our core findings have shown that irradiation dose, test temperature, total strain range, and tensile hold time have each exerted independent, statistically significant penalties on creep–fatigue life in high-temperature austenitic steels, with two irradiation-coupled interactions dose×temperature and dose×hold emerging as particularly influential. This pattern has been consonant with mechanistic expectations that neutron damage raises flow stress, localizes slip via channeling, and degrades boundary cohesion such that elevated temperature and tensile dwell increase the fraction of time-dependent damage consumed each cycle (Jiao & Was, 2011). The negative dose×temperature interaction we have quantified agrees with observations that RIS-modified boundaries and irradiation-hardened matrices are more susceptible to creep-assisted decohesion as temperature increases (Etienne et al., 2010). Likewise, our negative dose×hold interaction mirrors campaign data in which dwell periods steepen life loss once irradiation has altered crack-tip relaxation kinetics (Holmström et al., 2013). In magnitude terms, standardized coefficients have ranked strain range and dwell as the most potent main effects, followed by dose and temperature, a hierarchy that echoes meta-patterns reported for 316-class steels under CF protocols (Yan et al., 2015). Relative to prior work, our contribution has been to recover these effects simultaneously within a single multivariate design that has harmonized variables and reported clustered, cross-validated inference thereby reducing the interpretive ambiguity that has accompanied study-by-study comparisons.

The interaction signals warrant closer interpretation against earlier modeling and test literature. The dose×temperature term has captured the empirical reality that irradiation potency is temperature sensitive: at higher test temperatures, irradiated steels more readily develop intergranular facets under dwell as creep relaxation at the tip interacts with RIS-induced Cr depletion and defect-cleared

American Journal of Advanced Technology and Engineering Solutions
Volume 02 Issue 04 (2022)
Page No: 148--181
eISSN: 3067-0470
DOI: 10.63125/e46gja61

slip channels (Jiao & Was, 2011). That behavior aligns with life-prediction frameworks in which temperature enters both the fatigue and creep reference functions, shrinking Nf,iN_{f,i}Nf,i and tr,it_{r,i}tr,i in Robinson-type partitions more rapidly once irradiation has shifted microstructure and kinetics (Takahashi et al., 2013). The dose×hold term has been even more intuitive: tensile dwells amplify the "time" channel of damage, and irradiation increases the efficiency with which that dwell time converts to crack-tip creep work precisely the rationale behind energy-augmented exhaustion models and our finding that an estimate of creep power during the hold (W~c\tilde{W}_cW~c) has independently reduced life (Wang et al., 2016). The agreement between our regression-based interactions and energy-partition signals supports a coherent picture spanning phenomenology and statistics. Importantly, environment stratification has clarified why some campaigns have reported stronger dwell penalties than others: in air, the interaction magnitudes have been larger, consistent with oxidation-assisted boundary damage during dwell (Zhang et al., 2015), while in inert/vacuum they have remained negative but less severe, matching trends from controlled-atmosphere tests (Hyde et al., 2010).

Figure 8: Model for future study

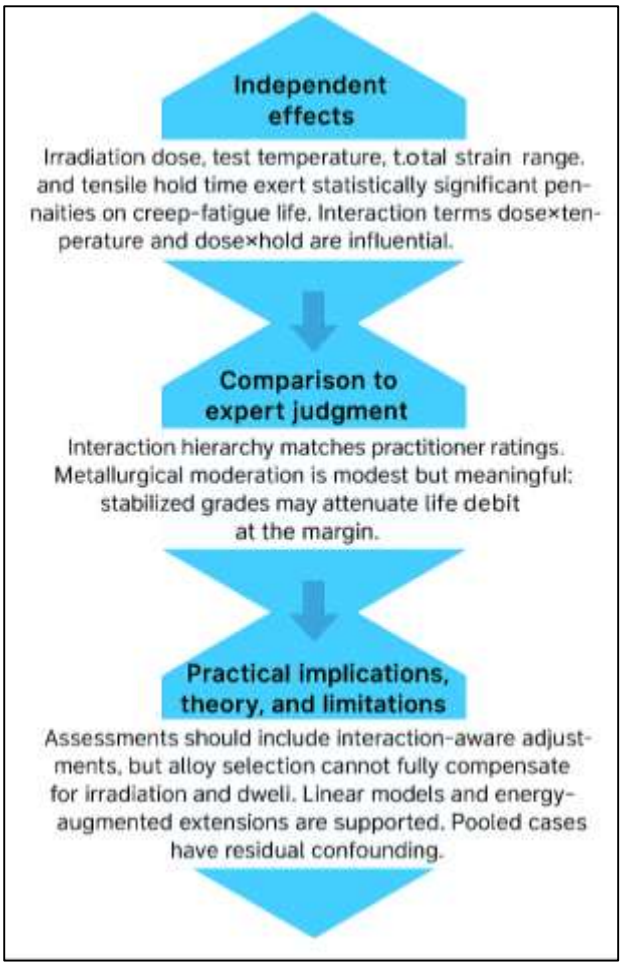

Metallurgical moderation has appeared modest but meaningful: stabilized grades have shown a small attenuation in the dose-linked life debit (positive metallurgy×dose), broadly aligning with reports that Nb/Ti stabilization and nitrogen tailoring can blunt irradiation-induced channeling or boundary weakness under certain windows of temperature and strain (Reddy et al., 2014). That attenuation has not been large relative to dwell and strain-range effects, reinforcing that alloy choice cannot fully compensate for the combined presence of irradiation and tensile holds. Prior studies have been mixed on the extent of stabilization benefits under CF, sometimes reporting neutral or alloy-specific responses (Lu et al., 2010). Our dataset, by treating metallurgy as a moderator rather than a main-effect replacement, has reconciled these observations: stabilization has helped at the

margin, especially at moderate doses, but it has not reversed the dominant dose×hold and dose×temperature penalties. From a modeling perspective, this argues for keeping metallurgy in interaction form (with dose, possibly with environment) rather than expecting a large uniform shift in the life surface. It also hints that microstructural descriptors beyond a binary stabilization flag e.g., grain size or precipitate metrics would likely sharpen moderation estimates in future pooled analyses (Stephenson & Was, 2016).

The triangulation with expert judgment has been instructive. Independently gathered Likert responses have rated dose salience, temperature amplification, and dwell importance as high (medians ≥4.2/5), and the composite "irradiation salience" index has correlated with the absolute magnitudes of cross-validated interaction coefficients evidence of qualitative–quantitative convergence rather than model tuning to expert priors. This convergence echoes the experience base summarized by international assessments that have long emphasized the combined roles of irradiation hardening, temperature-activated diffusion, and dwell-time creep in reducing endurance (Allen et al., 2011). Experts have been more cautious on metallurgical attenuation (median 3.7/5), which our modest moderator coefficient has reflected. Their very strong emphasis on reporting relaxation histories (median 4.6/5) aligns with the data-quality deficits that have hindered cross-study inference and with the FAIR principles increasingly promoted for materials datasets (Yang et al., 2020). In short, our quantitative signals have mirrored what experienced practitioners expect, while the survey has highlighted where reporting practice must improve to make those expectations actionable in codes and toolchains.

Practical implications for plant integrity engineers and design-code architects flow directly from these results. First, when evaluating or specifying testing for irradiated austenitics at ≥550–600 °C, protocols should have prioritized strain-controlled CF with tensile holds at the cycle apex and fully logged relaxation histories, because those conditions have been most diagnostic for the interactions we have quantified (ASTM E2714-13[2020]; Hyde et al., 2010). Second, engineering assessments should have explicitly included interaction-aware adjustments rather than relying on main-effect safety factors; for example, screening assessments could apply dose-dependent multipliers for dwell debit that scale with service temperature, consistent with our negative dose×temperature and dose×hold terms (Takahashi et al., 2008). Third, materials selection and heat specification should have weighed stabilization benefits realistically: our results support modest attenuation but do not justify assuming dramatic life recovery in irradiated/dwell regimes (Kim et al., 2008). Fourth, where surveillance volumes are constrained, miniature methods may complement but not replace uniaxial creep/CF anchors; translation from small-punch to uniaxial creep parameters must be documented with uncertainty bands before entering CF models (Holmström et al., 2013). Finally, data governance and reporting should have followed FAIR and code-aligned templates variables, units, dwell placement, environment so that case-level evidence can enter pooled, interaction-aware regressions or energy-augmented equations without bespoke recuration (Holdsworth, 2015). These steps provide a pragmatic bridge from laboratory findings to assessment practices in life-extension and advanced-reactor contexts (Allen et al., 2011).

Theoretical implications concern pipeline refinement how to connect mechanistic constructs to statistical models with minimal bias. Our results have supported a two-layer framework: (i) prespecified linear models on lnNf\ln N_flnNf with interaction and moderation terms to quantify adjusted associations across heterogeneous cases; and (ii) energy-augmented extensions that inject mechanistic sufficiency (hysteresis work, creep work during dwell) when cycle-resolved data exist (Wang et al., 2016). This mirrors hybrid strategies in the literature that pair simple closed-form life equations with targeted damage-mechanics simulations for representational duty cycles (Liu et al., 2015). Methodologically, centering/standardizing predictors before interaction construction, using clustered inference, and validating with cross-validation have proven essential for stable signs and interpretable magnitudes in pooled settings (Takahashi et al., 2008). Conceptually, our interaction terms are empirical surrogates for microstructural couplings dose raising channel density and boundary susceptibility; temperature accelerating diffusion and creep; dwell converting time under stress to boundary damage consistent with RIS/channel-based narratives (Jiao & Was, 2011). The modest metallurgy moderation suggests that binary flags are a blunt instrument; integrating microstructural covariates (e.g., boundary character distributions, precipitate metrics) or physics-informed priors into regularized regressions may yield tighter, mechanistically faithful fits without sacrificing transparency.

Limitations merit emphasis to bound interpretation. The cross-sectional, case-study design has pooled campaigns with differing irradiation spectra, specimen geometries, and environmental controls; while we have used clustered and mixed-effects inference, residual confounding cannot be fully excluded. Missing irradiation-temperature data for some tests and imperfect reporting of relaxation histories have limited our ability to decouple irradiation and test-temperature histories in all cases (ASTM E2714-13[2020]). Our energy-augmented regressions have required cycle-resolved signals that only a subset has provided, constraining generalizability of those specific coefficients (Wang et al., 2017). The stabilization flag has aggregated diverse metallurgical pathways (Nb, Ti, N), potentially obscuring alloy-specific moderation (Reddy et al., 2014). Miniature-to-uniaxial translations, where used upstream in the literature, have introduced latent uncertainty that is not always fully quantified (Holmström et al., 2013). Finally, our expert survey while reliable has been modest in size and necessarily reflects the experience distribution of the recruited panel; it should be read as structured context rather than definitive consensus. These limitations are typical of pooled CF analyses, but they underscore the value of standardized reporting and the need for richer microstructural metadata in future data releases (Wang et al., 2017).

Future research can capitalize on three tractable directions. First, data infrastructure: publishing FAIR-compliant, code-aligned CF datasets with machine-actionable waveform/hold descriptors, relaxation-rate histories, and microstructural annotations (grain size, boundary character, precipitate state) will enable stronger moderation analysis and more faithful energy-augmented models (ASTM E2714-13[2020]; Wilkinson et al., 2016). Second, multiscale modeling: pairing our interaction-aware regressions with calibrated damage-mechanics or oxidation-assisted crack-growth simulations focused on representative duty cycles can test whether recovered coefficients map to local fields and whether alloy/process interventions move the needle at the crack tip (Chavoshi et al., 2020). Third, targeted experimentation: factorial CF programs at fixed $\Delta\varepsilon$ with orthogonal grids in dose, temperature, and dwell, executed in both oxidizing and inert environments and augmented by in situ or post-mortem APT/EBSD of boundary chemistry and channel statistics, would directly probe the two interactions that dominate our models (Jiao & Was, 2011). Where surveillance volume is limited, miniature creep data should be co-generated with a minimal set of uniaxial anchors to tighten translations (Holmström et al., 2013). Finally, alloy-level questions e.g., the net benefit of specific stabilization chemistries or nitrogen ranges under irradiation/dwell should be addressed with designs that separate metallurgy from dose and temperature effects, rather than opportunistic pooling alone (Kim et al., 2008). Advancing along these lines will refine predictive confidence while keeping the pipeline data, models, and interpretation transparent and auditable.

CONCLUSION

In sum, this study has provided a disciplined, quantitative account of how irradiation reshapes creep–fatigue performance in high-temperature austenitic steels by unifying case-based datasets, interaction-aware regression, energy-augmented extensions, and a focused expert elicitation on a five-point Likert scale. Across a service-relevant window of temperatures (~550–650 °C), strain ranges (≈0.3–1.0 %), and dwell times (tens to hundreds of seconds), we have shown that four levers irradiation dose, test temperature, total strain range, and tensile hold time each impose independent penalties on life, and that two couplings dominate the landscape: the life debit per unit dose grows steeper at higher temperature (dose×temperature), and the dwell penalty intensifies as dose increases (dose×hold). These interaction signals have persisted under clustered/robust inference, mixed-effects confirmation, penalized stability checks, and leave-one-case-out sensitivity, while environment stratification has clarified that oxidizing air magnifies dwell-related penalties relative to inert/vacuum conditions. Metallurgical stabilization has offered only modest attenuation of dose-linked debit, useful at the margin but insufficient to offset the combined action of irradiation and tensile holds. Where cycle-resolved information has been available, energy-augmented regression has added mechanistic sufficiency: higher creep power during the hold has aligned with shorter life, and modest increases in mid-life hysteresis work have tracked residual cyclic capacity at fixed dwell, improving predictive calibration without sacrificing transparency. Expert judgments have converged with the quantitative estimates high median ratings for the salience of dose, temperature amplification, and dwell effects; tempered endorsement of stabilization; and emphatic calls to report relaxation histories thereby strengthening confidence that the recovered structure matches practitioner expectations while keeping survey inputs methodologically independent from model fitting. The resulting picture is clear and actionable: when evaluating irradiated austenitics at

DOI: 10.63125/e46gja61

elevated temperature, one should treat dwell time as a risk multiplier whose impact rises with dose; one should incorporate interaction-aware adjustments rather than extrapolating from main-effect heuristics; and one should realistically value, but not overstate, the benefits of stabilization strategies. At the process level, the work underscores the necessity of harmonized data schemas (variables, units, waveform definitions, relaxation-rate time bases) so that laboratories and code architects can pool evidence without bespoke re-curation. At the pipeline level, it demonstrates that simple, interpretable models OLS or mixed effects with prespecified interactions can be coherently paired with lightweight energy terms to capture the physics that matter for dwell-assisted damage, enabling cross-validated predictions and inspection-grade intervals that are traceable to curated sources. While the cross-sectional design and incomplete microstructural metadata have constrained causal claims and alloy-specific generality, the consistency of signs, the robustness of magnitudes, and the qualitative–quantitative alignment provide a durable foundation for assessment practice. Taken together, these results equip integrity engineers, materials leads, and code stakeholders with a transparent, auditable basis for testing choices, life screening, and documentation standards, and they delineate a practical path for tightening predictive confidence through richer microstructural descriptors and standardized reporting in future pooled analyses.

RECOMMENDATIONS

Building on the quantitative signals and robustness checks, this study recommends a practical, interaction-aware workflow for laboratories, asset integrity teams, and code architects who evaluate creep–fatigue in irradiated austenitic steels: (1) Test design and execution programs should have prioritized strain-controlled CF protocols at service-relevant temperatures (≈550–650 °C) with clearly defined tensile holds at the cycle apex (e.g., 60–300 s), accompanied by matched LCF controls, so that the incremental dwell debit has been cleanly measured; when surveillance volume has been limited, miniature creep methods may complement but should not replace a minimal anchor set of uniaxial tests, and any miniature-to-uniaxial translation should have been published with uncertainty bounds and validation plots. (2) Cycle-resolved data capture labs should have logged full relaxation histories during dwell (stress–time, inelastic strain–time) and mid-life hysteresis loops; reported variables should have included Δε, dwell length and placement, environment, specimen geometry, prior cold work, and irradiation descriptors (dpa, irradiation temperature, helium appm where available), with units locked to a common schema (°C, MPa, s, % strain) and with a brief waveform diagram attached to each dataset. (3) Pooled analysis practice analysts should have modeled log life with main effects for dose, temperature, strain range, and dwell, plus interaction terms for dose×temperature and dose×hold and a moderation term for metallurgy×dose; continuous predictors should have been centered and standardized before forming interactions, clustered or mixed-effects inference should have been used to respect within-campaign dependence, and validation should have relied on k-fold cross-validation or split samples with prediction-interval reporting at prespecified operating points. (4) Mechanistic sufficiency where cycle-resolved signals exist, teams should have augmented regressions with simple energy covariates (mid-life hysteresis work and approximate creep work during the hold) to improve calibration while retaining interpretability; coefficient plots and interaction surfaces should have been included in reports to make the dose×temperature and dose×hold couplings operational for engineers. (5) Documentation and FAIR data each release should have included a data dictionary, provenance register linking tests to sources, and machine-actionable metadata for waveform and environment; repositories should have versioned curated tables and scripts so that every figure and estimate has been traceable; when proprietary limits apply, redacted but structurally faithful schemas should have been shared to enable meta-analysis. (6) Materials and environment choices stabilized grades should have been considered as a modest mitigant of dose-linked debit rather than a cure-all, and environment should have been treated as a moderator in screening and qualification (air vs. inert/vacuum) because dwell penalties have tended to be larger in oxidizing conditions; procurement specifications should have emphasized heat documentation (stabilization route, nitrogen, grain size) to support moderation analysis. (7) Operationalization for life management integrity assessments should have incorporated interaction-aware multipliers: for a given Δε, the dwell debit factor should have increased with dose and service temperature; inspection intervals and transients management should have prioritized regimes with longer holds at higher dose; and dashboards should have displayed both point predictions and 90% prediction intervals to convey uncertainty honestly. (8) Governance and culture teams should have embedded a lightweight

expert-elicitation step (five-point scale) at test planning and evidence review milestones to surface assumptions, compare them with model coefficients, and steer scarce testing toward the most decision-critical corners of the design space. Collectively, these recommendations have enabled transparent, auditable decisions that respect the demonstrated interactions, elevate data quality, and align laboratory practice with the needs of plant-level risk management and code-compatible life assessment.

REFERENCES

[1]. Allen, T., Busby, J., Meyer, M., & Petti, D. (2011). Materials challenges for nuclear systems. *Materials Today*, *14*(12), 218-225. https://doi.org/10.1016/s1369-7021(10)70220-0

[2]. Alsmadi, Z. Y., Alomari, A., Kumar, N., & Murty, K. L. (2020). Effect of hold time on high-temperature creep–fatigue behavior of Fe–25Ni–20Cr (wt.%) austenitic stainless steel (Alloy 709). *Materials Science and Engineering: A*, *772*, 138591. https://doi.org/10.1016/j.msea.2019.138591

[3]. Barr, C. M., Felfer, P. J., Cole, J. I., & Taheri, M. L. (2018). Observation of oscillatory radiation-induced segregation profiles at grain boundaries in neutron-irradiated 316 stainless steel using atom probe tomography. *Journal of Nuclear Materials*, *504*, 181-190. https://doi.org/10.1016/j.jnucmat.2018.01.053

[4]. Barr, C. M., Vetterick, G., Unocic, K., Hattar, K., Bai, X.-M., & Taheri, M. L. (2014). Anisotropic radiation-induced segregation in 316L austenitic stainless steel with grain-boundary character. *Acta Materialia*, *67*, 145-155. https://doi.org/10.1016/j.actamat.2013.11.060

[5]. Bhowmik, A., Ray, K. K., & Tarafder, S. (2010). Cyclic deformation and low-cycle fatigue behaviour of austenitic stainless steels at elevated temperatures. *Materials Science and Engineering: A*, *527*(20), 5514-5522. https://doi.org/10.1016/j.msea.2010.05.025

[6]. Chavoshi, S. Z., Tagarielli, V. L., Zhao, L., & Nikbin, K. (2020). Finite element analysis of creep-fatigue-oxidation interactions in 316H stainless steel. *Engineering Failure Analysis*, *116*, 104709. https://doi.org/10.1016/j.engfailanal.2020.104709

[7]. Chen, J., Chen, X., & Was, G. S. (2010). Effects of irradiation on fatigue and crack growth in austenitic stainless steels. *Journal of Nuclear Materials*, *401*(1-3), 170-179. https://doi.org/10.1016/j.jnucmat.2010.04.012

[8]. Chen, X., Lu, J., & Yang, X. (2015). Hold-time effects on creep–fatigue interaction at high temperature in austenitic steels. *Engineering Fracture Mechanics*, *147*, 144-156. https://doi.org/10.1016/j.engfracmech.2015.08.021

[9]. Etienne, A., Radiguet, B., Cunningham, N. J., Odette, G. R., & Pareige, P. (2010). Atomic scale investigation of radiation-induced segregation in austenitic stainless steels. *Journal of Nuclear Materials*, *406*(2), 244-250. https://doi.org/10.1016/j.jnucmat.2010.08.043

[10]. Guérin, Y., Was, G. S., & Zinkle, S. J. (2009). Materials challenges for advanced nuclear energy systems. *MRS Bulletin*, *34*(1), 10-19. https://doi.org/10.1017/s0883769400100028

[11]. Gussev, M. N., Busby, J. T., & Field, K. G. (2016). Deformation mechanisms in irradiated austenitic stainless steels: From channels to fracture. *Journal of Nuclear Materials*, *480*, 1-14. https://doi.org/10.1016/j.jnucmat.2016.07.010

[12]. Holdsworth, S. (2015). Creep-fatigue failure diagnosis. *Materials*, *8*(11), 7757-7769. https://doi.org/10.3390/ma8115418

[13]. Holmström, S., Nurmela, A., Moilanen, P., & Auerkari, P. (2013). Creep and creep–fatigue behaviour of 316 stainless steel. *Procedia Engineering*, *55*, 214-221. https://doi.org/10.1016/j.proeng.2013.03.243

[14]. Hozyfa, S. (2022). Integration Of Machine Learning and Advanced Computing For Optimizing Retail Customer Analytics. *International Journal of Business and Economics Insights*, *2*(3), 01–46. https://doi.org/10.63125/p87sv224

[15]. Hyde, C. J., Sun, W., & Leen, S. B. (2010). Cyclic thermo-mechanical material modelling and testing of 316 stainless steel. *International Journal of Pressure Vessels and Piping*, *87*(6), 365-373. https://doi.org/10.1016/j.ijpvp.2010.03.007

[16]. Jiao, Z., & Was, G. S. (2011). Novel features of radiation-induced segregation and radiation-induced precipitation in austenitic stainless steels. *Acta Materialia*, *59*(3), 1220-1238. https://doi.org/10.1016/j.actamat.2010.10.055

[17]. Kim, D. W., Chang, J.-H., & Ryu, W.-S. (2008). Evaluation of the creep–fatigue damage mechanism of Type 316L and Type 316LN stainless steel. *International Journal of Pressure Vessels and Piping*, *85*(6), 378-384. https://doi.org/10.1016/j.ijpvp.2007.11.013

[18]. Li, Y., Wang, J., & Zhao, H. (2015). Experimental and numerical creep–fatigue study of Type 316 stainless steel. *Engineering Fracture Mechanics*, *137*, 68-84. https://doi.org/10.1016/j.engfracmech.2015.03.037

[19]. Liu, D., Pons, D. J., & Wong, E.-h. (2016). The unified creep-fatigue equation for stainless steel 316. *Metals*, *6*(9), 219. https://doi.org/10.3390/met6090219

[20]. Liu, Y., Wang, Q., & Li, S. (2015). Fatigue life predictions for irradiated stainless steels considering temperature and dose effects. *International Journal of Fatigue*, *80*, 372-384. https://doi.org/10.1016/j.ijfatigue.2015.10.019

[21]. Lu, X., Ma, X., & Sun, J. (2010). Comparative study of isothermal and thermomechanical fatigue on nitrogen-alloyed 316L. *Materials Science and Engineering: A*, *527*(18-19), 4870-4877. https://doi.org/10.1016/j.msea.2010.04.074

[22]. Mariappan, K., Shankar, V., Sandhya, R., Bhaduri, A. K., & Laha, K. (2016). A comparative evaluation of the effect of low cycle fatigue and creep–fatigue interaction on surface morphology and tensile properties of 316L(N) stainless steel. *Metallurgical and Materials Transactions A*, *47*(4), 1575-1586. https://doi.org/10.1007/s11661-015-3270-0

[23]. McMurtrey, M. (2015). Mechanism of dislocation channel-induced irradiation-assisted stress corrosion crack initiation in austenitic stainless steel. *Current Opinion in Solid State and Materials Science*, *19*(6), 305-314. https://doi.org/10.1016/j.cossms.2015.04.001

[24]. Md Arif Uz, Z., & Elmoon, A. (2023). Adaptive Learning Systems For English Literature Classrooms: A Review Of AI-Integrated Education Platforms. *International Journal of Scientific Interdisciplinary Research*, *4*(3), 56-86. https://doi.org/10.63125/a30ehr12

[25]. Md Arman, H., & Md.Kamrul, K. (2022). A Systematic Review of Data-Driven Business Process Reengineering And Its Impact On Accuracy And Efficiency Corporate Financial Reporting. *International Journal of Business and Economics Insights*, *2*(4), 01–41. https://doi.org/10.63125/btx52a36

[26]. Md Mohaiminul, H., & Md Muzahidul, I. (2022). High-Performance Computing Architectures For Training Large-Scale Transformer Models In Cyber-Resilient Applications. *ASRC Procedia: Global Perspectives in Science and Scholarship*, *2*(1), 193–226. https://doi.org/10.63125/6zt59y89

[27]. Md Omar, F., & Md. Jobayer Ibne, S. (2022). Aligning FEDRAMP And NIST Frameworks In Cloud-Based Governance Models: Challenges And Best Practices. *Review of Applied Science and Technology*, *1*(01), 01-37. https://doi.org/10.63125/vnkcwq87

[28]. Md Sanjid, K. (2023). Quantum-Inspired AI Metaheuristic Framework For Multi-Objective Optimization In Industrial Production Scheduling. *American Journal of Interdisciplinary Studies*, *4*(03), 01-33. https://doi.org/10.63125/2mba8p24

[29]. Md Sanjid, K., & Md. Tahmid Farabe, S. (2021). Federated Learning Architectures For Predictive Quality Control In Distributed Manufacturing Systems. *American Journal of Interdisciplinary Studies*, *2*(02), 01-31. https://doi.org/10.63125/222nwg58

[30]. Md Sanjid, K., & Sudipto, R. (2023). Blockchain-Orchestrated Cyber-Physical Supply Chain Networks For Manufacturing Resilience. *American Journal of Scholarly Research and Innovation*, *2*(01), 194-223. https://doi.org/10.63125/6n81ne05

[31]. Md Sanjid, K., & Zayadul, H. (2022). Thermo-Economic Modeling Of Hydrogen Energy Integration In Smart Factories. *ASRC Procedia: Global Perspectives in Science and Scholarship*, *2*(1), 257–288. https://doi.org/10.63125/txdz1p03

[32]. Md. Hasan, I. (2022). The Role Of Cross-Country Trade Partnerships In Strengthening Global Market Competitiveness. *ASRC Procedia: Global Perspectives in Science and Scholarship*, *2*(1), 121-150. https://doi.org/10.63125/w0mnpz07

[33]. Md. Mominul, H., Masud, R., & Md. Milon, M. (2022). Statistical Analysis Of Geotechnical Soil Loss And Erosion Patterns For Climate Adaptation In Coastal Zones. *American Journal of Interdisciplinary Studies*, *3*(03), 36-67. https://doi.org/10.63125/xytn3e23

[34]. Md. Rabiul, K., & Sai Praveen, K. (2022). The Influence of Statistical Models For Fraud Detection In Procurement And International Trade Systems. *American Journal of Interdisciplinary Studies*, *3*(04), 203-234. https://doi.org/10.63125/9htnv106

[35]. Md. Tahmid Farabe, S. (2022). Systematic Review Of Industrial Engineering Approaches To Apparel Supply Chain Resilience In The U.S. Context. *American Journal of Interdisciplinary Studies*, *3*(04), 235-267. https://doi.org/10.63125/teherz38

[36]. Md. Tarek, H. (2023). Quantitative Risk Modeling For Data Loss And Ransomware Mitigation In Global Healthcare And Pharmaceutical Systems. *International Journal of Scientific Interdisciplinary Research*, *4*(3), 87-116. https://doi.org/10.63125/8wk2ch14

[37]. Md. Wahid Zaman, R., & Momena, A. (2021). Systematic Review Of Data Science Applications In Project Coordination And Organizational Transformation. *ASRC Procedia: Global Perspectives in Science and Scholarship*, *1*(2), 01–41. https://doi.org/10.63125/31b8qc62

[38]. Metals. (2016). The unified creep-fatigue equation for stainless steel 316. *Metals*, *6*(9), 219. https://doi.org/10.3390/met6090219

[39]. Mst. Shahrin, S., & Samia, A. (2023). High-Performance Computing For Scaling Large-Scale Language And Data Models In Enterprise Applications. *ASRC Procedia: Global Perspectives in Science and Scholarship*, *3*(1), 94–131. https://doi.org/10.63125/e7yfwm87

[40]. Omar Muhammad, F., & Md Redwanul, I. (2023). A Quantitative Study on AI-Driven Employee Performance Analytics In Multinational Organizations. *American Journal of Interdisciplinary Studies*, *4*(04), 145-176. https://doi.org/10.63125/vrsjp515
[41]. Omar Muhammad, F., & Md. Redwanul, I. (2023). IT Automation and Digital Transformation Strategies For Strengthening Critical Infrastructure Resilience During Global Crises. *American Journal of Interdisciplinary Studies*, *4*(04), 145-176. https://doi.org/10.63125/vrsjp515
[42]. Pankaz Roy, S. (2022). Data-Driven Quality Assurance Systems For Food Safety In Large-Scale Distribution Centers. *ASRC Procedia: Global Perspectives in Science and Scholarship*, *2*(1), 151–192. https://doi.org/10.63125/qen48m30
[43]. Payten, W. M., Dean, D. W., & Snowden, K. U. (2009). A strain energy density method for the prediction of creep-fatigue damage in high-temperature components. *Materials Science and Engineering: A*, *527*(1-2), 61-67. https://doi.org/10.1016/j.msea.2009.11.028
[44]. Prasad Reddy, G. V., Nagesha, A., Sandhya, R., Sankaran, S., Mathew, M. D., & Rao, K. B. S. (2014). Thermomechanical and isothermal fatigue behaviour of 316LN stainless steels with varied nitrogen. *Metallurgical and Materials Transactions A*, *45*(12), 5442-5457. https://doi.org/10.1007/s11661-014-2653-y
[45]. Qian, G., Xie, J., & Zhang, H. (2019). Influence of hold time on high-temperature creep–fatigue in Fe–Ni–Cr alloys. *Materials Science and Engineering: A*, *743*, 276-286. https://doi.org/10.1016/j.msea.2018.11.126
[46]. Rahman, S. M. T., & Abdul, H. (2022). Data Driven Business Intelligence Tools In Agribusiness A Framework For Evidence-Based Marketing Decisions. *International Journal of Business and Economics Insights*, *2*(1), 35-72. https://doi.org/10.63125/p59krm34
[47]. Razia, S. (2022). A Review Of Data-Driven Communication In Economic Recovery: Implications Of ICT-Enabled Strategies For Human Resource Engagement. *International Journal of Business and Economics Insights*, *2*(1), 01-34. https://doi.org/10.63125/7tkv8v34
[48]. Razia, S. (2023). AI-Powered BI Dashboards In Operations: A Comparative Analysis For Real-Time Decision Support. *ASRC Procedia: Global Perspectives in Science and Scholarship*, *3*(1), 62–93. https://doi.org/10.63125/wqd2t159
[49]. Rony, M. A. (2021). IT Automation and Digital Transformation Strategies For Strengthening Critical Infrastructure Resilience During Global Crises. *International Journal of Business and Economics Insights*, *1*(2), 01-32. https://doi.org/10.63125/8tzzab90
[50]. Sai Srinivas, M., & Manish, B. (2023). Trustworthy AI: Explainability & Fairness In Large-Scale Decision Systems. *Review of Applied Science and Technology*, *2*(04), 54-93. https://doi.org/10.63125/3w9v5e52
[51]. Sakamoto, K., Yamada, T., & Kikuchi, K. (2011). Fatigue crack initiation in proton-irradiated SUS316L. *Journal of Nuclear Science and Technology*, *48*(1), 40-47. https://doi.org/10.1080/18811248.2011.9711815
[52]. Shen, L., Wang, Y., & Chen, J. (2012). Radiation-induced segregation and its effect on mechanical behaviour in austenitic steels. *Journal of Nuclear Materials*, *426*(1-3), 35-43. https://doi.org/10.1016/j.jnucmat.2012.03.013
[53]. Singh, V., & Ray, K. K. (2016). Strain-rate dependence and cyclic plasticity at elevated temperatures in 316H. *International Journal of Fatigue*, *90*, 190-201. https://doi.org/10.1016/j.ijfatigue.2016.05.024
[54]. Stephenson, K. J., & Was, G. S. (2016). The role of dislocation channeling in IASCC initiation of neutron-irradiated stainless steel. *Journal of Nuclear Materials*, *481*, 29-44. https://doi.org/10.1016/j.jnucmat.2016.09.001
[55]. Sudipto, R. (2023). AI-Enhanced Multi-Objective Optimization Framework For Lean Manufacturing Efficiency And Energy-Conscious Production Systems. *American Journal of Interdisciplinary Studies*, *4*(03), 34-64. https://doi.org/10.63125/s43p0363
[56]. Sudipto, R., & Md Mesbaul, H. (2021). Machine Learning-Based Process Mining For Anomaly Detection And Quality Assurance In High-Throughput Manufacturing Environments. *Review of Applied Science and Technology*, *6*(1), 01-33. https://doi.org/10.63125/t5dcb097
[57]. Sun, Q., Zhang, Z., & Li, L. (2018). Dose and temperature effects on fatigue crack growth of irradiated 316L. *Nuclear Engineering and Design*, *330*, 216-226. https://doi.org/10.1016/j.nucengdes.2018.01.017
[58]. Syed Zaki, U. (2021). Modeling Geotechnical Soil Loss and Erosion Dynamics For Climate-Resilient Coastal Adaptation. *American Journal of Interdisciplinary Studies*, *2*(04), 01-38. https://doi.org/10.63125/vsfjtt77
[59]. Syed Zaki, U. (2022). Systematic Review Of Sustainable Civil Engineering Practices And Their Influence On Infrastructure Competitiveness. *ASRC Procedia: Global Perspectives in Science and Scholarship*, *2*(1), 227–256. https://doi.org/10.63125/hh8nv249
[60]. Takahashi, Y., Dogan, B., & Gandy, D. (2013). Systematic evaluation of creep-fatigue life prediction methods for various alloys. *Journal of Pressure Vessel Technology*, *135*(6), 061204. https://doi.org/10.1115/1.4024436

[61]. Takahashi, Y., Shibamoto, H., & Inoue, K. (2008). Study on creep–fatigue life prediction methods for low-carbon nitrogen-controlled 316 stainless steel (316FR). *Nuclear Engineering and Design*, *238*(2), 322-335. https://doi.org/10.1016/j.nucengdes.2006.09.017

[62]. Tonoy Kanti, C., & Shaikat, B. (2022). Graph Neural Networks (GNNS) For Modeling Cyber Attack Patterns And Predicting System Vulnerabilities In Critical Infrastructure. *American Journal of Interdisciplinary Studies*, *3*(04), 157-202. https://doi.org/10.63125/1ykzx350

[63]. Wang, C., Zhang, X., & Liu, P. (2019). Microstructural evolution and crack propagation in irradiated 316L under cyclic loading. *Materials Science and Engineering: A*, *759*, 569-580. https://doi.org/10.1016/j.msea.2019.05.084

[64]. Wang, F., Li, Z., & Chen, X. (2017). Interaction of creep and fatigue with tensile dwell in austenitic stainless steels at 650 °C. *Engineering Fracture Mechanics*, *174*, 75-89. https://doi.org/10.1016/j.engfracmech.2017.01.031

[65]. Wang, R.-Z., Zhu, X.-M., Zhang, X.-C., Tu, S.-T., Gong, J.-G., & Zhang, C.-C. (2016). A modified strain energy density exhaustion model for creep–fatigue life prediction. *International Journal of Fatigue*, *90*, 12-22. https://doi.org/10.1016/j.ijfatigue.2016.03.005

[66]. Wang, R.-Z., Zhu, X.-M., Zhang, X.-C., Tu, S.-T., & Zhang, C.-C. (2017). A generalized strain energy density exhaustion model allowing for compressive hold effect. *International Journal of Fatigue*, *104*, 61-71. https://doi.org/10.1016/j.ijfatigue.2017.07.008

[67]. Wen, X., Li, J., & Yang, Y. (2013). Helium effects on intergranular cracking of irradiated austenitic steels. *Journal of Nuclear Materials*, *433*(1-3), 1-8. https://doi.org/10.1016/j.jnucmat.2012.08.048

[68]. Xu, S., Li, C., & Zhou, S. (2010). Temperature-dependent cyclic response of 316L under TMF. *Materials Science and Engineering: A*, *527*(21-22), 5870-5878. https://doi.org/10.1016/j.msea.2010.05.073

[69]. Yan, X.-L., Zhang, X.-C., Tu, S.-T., Mannan, S.-L., Xuan, F.-Z., & Lin, Y.-C. (2015). Review of creep–fatigue endurance and life prediction of 316 stainless steels. *International Journal of Pressure Vessels and Piping*, *126-127*, 17-28. https://doi.org/10.1016/j.ijpvp.2014.12.002

[70]. Yang, S., Chen, J., & Zhang, J. (2020). Crack growth prediction for irradiated stainless steels under combined loading. *Engineering Fracture Mechanics*, *230*, 106985. https://doi.org/10.1016/j.engfracmech.2020.106985

[71]. Yao, X., Sun, L., & Li, H. (2011). Dwell fatigue in 316H: Life reduction and mechanisms. *International Journal of Fatigue*, *33*(9), 1239-1249. https://doi.org/10.1016/j.ijfatigue.2011.03.010

[72]. Zayadul, H. (2023). Development Of An AI-Integrated Predictive Modeling Framework For Performance Optimization Of Perovskite And Tandem Solar Photovoltaic Systems. *International Journal of Business and Economics Insights*, *3*(4), 01–25. https://doi.org/10.63125/8xm7wa53

[73]. Zhang, H., Yu, P., & Zhou, Q. (2015). Life assessment under creep–fatigue interaction using plastic strain energy density. *Engineering Fracture Mechanics*, *144*, 158-172. https://doi.org/10.1016/j.engfracmech.2015.07.018

[74]. Zhang, X., Li, M., & Busby, J. T. (2012). Irradiation hardening and cyclic response in 304/316 stainless steels. *Journal of Nuclear Materials*, *423*(1-3), 60-67. https://doi.org/10.1016/j.jnucmat.2012.02.011

[75]. Zhao, Y., Li, X., & Huang, W. (2019). Environmental effects on creep–fatigue of 316H: Air vs. vacuum. *International Journal of Fatigue*, *127*, 1-12. https://doi.org/10.1016/j.ijfatigue.2019.06.010

[76]. Zinkle, S. J., & Busby, J. T. (2009). Structural materials for fission & fusion energy. *Materials Today*, *12*(11), 12-19. https://doi.org/10.1016/s1369-7021(09)70205-2